Advances in Colloid and Interface Science 355 (2026) 103913

Contents lists available at ScienceDirect

Advances in Colloid and Interface Science

journal homepage: www.elsevier.com/locate/cis

Modelling the impact of temperature on nanocarrier behavior: Thermodynamics, structural transitions, and drug release

Marcello Schifone [1], Giuseppe Nunziata [1], Filippo Rossi [*]

Department of Chemistry, Materials and Chemical Engineering "Giulio Natta", Politecnico di Milano, Piazza Leonardo da Vinci 32, 20133 Milan, Italy

ARTICLE INFO

Keywords:
Thermo-responsive
Nanoparticles
Drug release
Modelling
Thermodynamics

ABSTRACT

Thermo-responsive polymeric nanoparticles represent one of the most powerful classes of smart drug delivery systems, thanks to their ability to translate temperature variations into precisely regulated drug-release responses. Unlike conventional carriers, where temperature acts merely as a kinetic accelerator, thermo-responsive nanocarriers exploit temperature as an active control parameter capable of inducing structural, thermodynamic, and transport transitions within the delivery system. The release for these systems can be rationally modulated through three fundamental mechanisms: temperature-accelerated degradation and erosion of biodegradable matrices, temperature-dependent transport processes governed by diffusion and solubility, and switch-like release triggered by thermo-induced structural transitions such as lower critical solution temperature (LCST)/upper critical solution temperature (UCST)-driven polymer collapse or lipid bilayer melting. This work critically examines how temperature alters carrier architecture, polymer-solvent interactions, and internal transport pathways, and how these changes can be explicitly captured through mathematical modelling. Empirical, semi-empirical, and fully mechanistic modelling frameworks are systematically discussed, highlighting their strengths, limitations, and physical interpretability. Particular emphasis is placed on models that couple temperature to nanoparticle geometry, polymer thermodynamics, and diffusion dynamics, enabling a predictive description of release behavior and continuous modulation regimes. This article proposes a rational design for next-generation thermo-responsive nanocarriers, in which polymer chemistry, nanoparticle structure, experimental characterization, and mechanistic modelling are integrated from the earliest stages of material development. By unifying thermo-responsive material design with physically meaningful release models, this review aims to provide both a conceptual framework and a practical toolbox for the development of smart nanomedicines whose temperature-dependent behavior can be predicted.

1. Introduction

The use of nanoscale devices as drug delivery systems (DDSs) has become a major focus in biomedical research [1–3]. Particular attention has been directed toward hydrogels [4,5], polymeric microspheres [6,7], and nanoparticles [2,8] as carriers for cell-specific targeting and "smart" drug delivery [9]. Modern DDSs are increasingly engineered to minimize or eliminate systemic side effects and maximize therapeutic efficacy by operating within the drug's therapeutic window [10,11], defined as the concentration range between the minimum effective level (C_{min}) and the maximum tolerable level (C_{max}) [12]. Within this context, stimuli-responsive nanocontainers (NCs) have emerged as one of the most promising classes of DDSs to achieve controlled drug release [13]. The efficiency of stimuli-responsive NCs lies in their ability to exhibit adaptive behaviors such as altering their aggregation state, undergoing chemical transformations, or displaying volume phase transitions in response to environmental changes [14]. This "smart" behavior allows them to release the appropriate dose of drug only when and where required, reducing off-target effects and improving overall treatment outcomes [15]. External triggers can be classified into physical [16] and chemical stimuli [17]. Physical stimuli include temperature, light, ultrasound, and magnetic or electric fields, whereas chemical stimuli involve variations in pH, ionic strength, or the presence of specific biomolecules or chemical agents [18]. Fig. 1 shows the most common physical and chemical stimuli employed in drug delivery to achieve "smart" release behavior.

* Corresponding author.
E-mail address: filippo.rossi@polimi.it (F. Rossi).
[1] Equal contribution.

https://doi.org/10.1016/j.cis.2026.103913
Received in revised form 24 April 2026;
Available online 29 April 2026

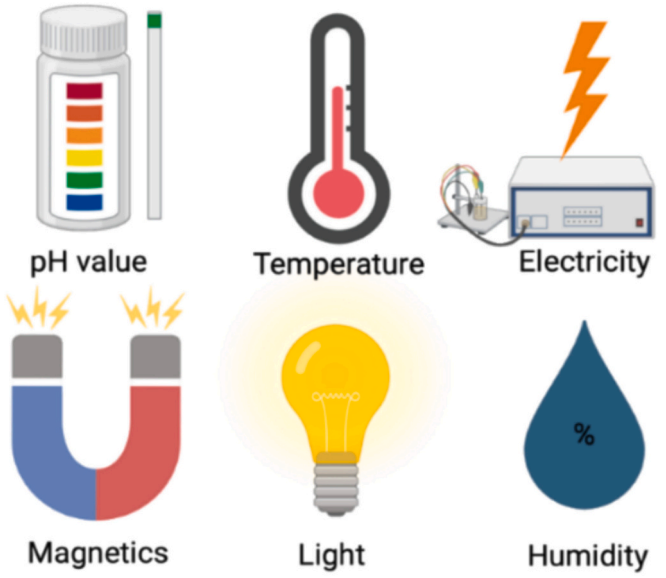

Fig. 1. Physical and chemical stimuli for drug release. Reprinted with permission from [19].

Temperature-sensitive DDSs are among them the most extensively studied types of stimuli-responsive formulations [19,20]. Temperature-dependence can dictate the behavior of DDSs in a broad spectrum of possibilities to trigger drug release. A first important category comprises biodegradable DDSs, in which drug release is governed by the progressive degradation of the carrier material [21,22]. In these systems, temperature does not act as an on–off trigger associated with a critical transition temperature [23]. Instead, increasing the incubation temperature accelerates the degradation kinetics of the delivery system accelerates, leading to a correspondingly faster release of the encapsulated drug [24]. Polymers commonly employed in biodegradable DDSs include natural materials such as chitosan [25,26], alginate [27,28], hyaluronic acid [29], as well as synthetic ones like polycaprolactone (PCL) [30], poly lactic acid (PLA) [31,32] and poly(lactic-co-glycolic acid) (PLGA) [33]. Another widely studied class of temperature-dependent DDSs is based on thermo-responsive polymers, which undergo reversible physical or chemical changes in response to temperature variations within the physiological range. Commonly used polymers in this context include poly(N-isopropylacrylamide) (PNIPAM) [34,35], poly(ethylene glycol) (PEG) based polymers [36,37], poly(oligo(ethylene glycol) methacrylate) (POEGMA) [38]. Importantly, many of these temperature-responsive polymers are used as building blocks for polymeric nanoparticles, particularly amphiphilic block copolymers that self-assemble into supramolecular structures in aqueous environments composed of a hydrophobic core and a hydrophilic shell [39,40]. In this core-shell configuration, the core serves as a reservoir for the therapeutic agent, while the surrounding polymeric shell functions as a protective barrier against chemical degradation, enzymatic attack, and mechanical stress [41]. The hydrophobic core enables high drug-loading efficiency, whereas the hydrophilic shell ensures colloidal stability in physiological media and regulates drug release kinetics by providing specific properties such as Lower Critical Solution Temperature (LCST) or Upper Critical Solution Temperature (UCST) behavior [42]. Although drugs may localize in both compartments, the core remains the predominant site of encapsulation [43].

Overall, this two-layered organization enhances drug-loading capacity and enables precise temporal and spatial control over drug release [44]. A further prominent class of temperature-sensitive DDSs is represented by thermo-sensitive liposomes (TSLs) [45]. In these systems, temperature directly regulates drug release through the lipid bilayer phase transition occurring at the melting temperature (T_m) [46]. When the temperature increases beyond T_m, the membrane undergoes a transition from a rigid gel phase to a liquid-crystalline phase, leading to a pronounced increase in bilayer fluidity and permeability [47,48]. Fig. 2 and Table 1 provide a schematic overview of the release mechanisms discussed above.

To regulate and optimize drug delivery from these carriers over time, it is essential to study drug release profiles, which describe the kinetics of drug diffusion from the nanoparticle into the external medium [49]. These processes can be accurately reproduced through in vitro experiments [50,51].

DDSs should not be regarded as a “black boxes” but as a physical systems in which drug release occurs through one or more well-defined mechanisms [52]. These may include diffusion [53], polymer erosion [54,55], matrix degradation [56–58], and biological absorption or uptake [59,60]. Mathematical and computational modelling plays a crucial role in enhancing the understanding of drug delivery systems by elucidating how different mechanisms and design parameters influence drug release [61]. Predictions derived from in silico studies can be used to optimize the formulation, geometry, and manufacturing process of the final dosage form [62,63]. Mathematical models help predict the rate, extent, and mechanisms of drug release from delivery systems, thereby accelerating the development of optimal pharmaceutical formulations by reducing the need for extensive experimental testing [64,65]. In this context, mathematical models are generally classified as either empirical/semi-empirical or mechanistic [52]. Empirical and semi-empirical models often lead to relatively simple mathematical expressions, they typically describe drug release through power-law equations where the exponent provides insight into the underlying release mechanism [66,67]. In contrast, mechanistic models have gained increasing attention due to their ability to incorporate complex physicochemical phenomena [68,69]. These models account for multiple coupled processes using fundamental balance equations and parameters with explicit physical and chemical meaning [70]. This facilitates a direct connection between model variables and the intrinsic temperature-dependence of the drug carrier. The aim of this review is to provide a comprehensive and mechanistically grounded overview of the most commonly employed DDSs whose behavior is related to temperature, with particular emphasis on how temperature governs drug release through well-defined physicochemical mechanisms. Rather than treating temperature simply as an external parameter that accelerates or slows down release kinetics, this work focuses on clarifying the role of temperature as an active driving force of structural, thermodynamic, and transport phenomena within the carrier.

Representative classes of temperature-dependent DDSs are examined, with attention dedicated to identify how temperature influences drug transport with particular emphasis placed on temperature-induced structural transitions of the delivery system (e.g., matrix degradation, changes in nanoparticle size or shell thickness, phase transitions in lipid bilayers) and on the thermodynamic principles that govern these transformations when relevant. Beyond describing the underlining mechanisms of drug release, a central aim is to critically analyze the state of the art in mathematical modelling of temperature-dependent drug release. For each DDS considered, the most relevant empirical, semi-empirical or mechanistic model available in the literature are discussed, with a specific focus on how temperature is incorporated into the governing equations whether through kinetic laws, thermodynamic parameters, structural descriptors, or coupled transport processes. While numerous studies address either thermo-responsive materials or mathematical models of drug release, the explicit connection between temperature-driven structural and thermodynamic changes in DDSs and their mathematical description remains fragmented across the literature. One of the key contributions of this work is therefore to bring these elements together within a unified conceptual framework. In this sense, the novelty of the present review lies in establishing clear, physically meaningful links between temperature, carrier structure, thermodynamics, and drug-release modelling across different classes of DDSs. By

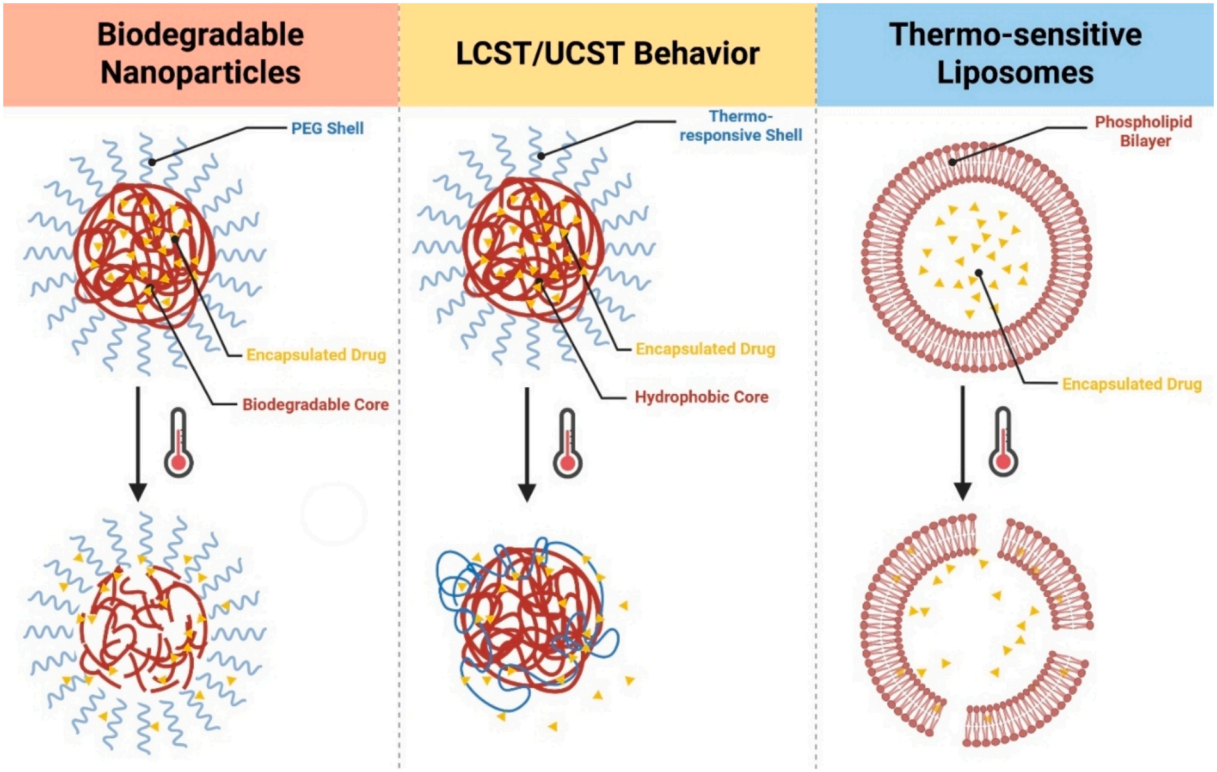

Fig. 2. Temperature-dependent mechanisms of drug release from nanocarriers.

Table 1
Comparative overview of temperature effects on drug delivery systems: mechanisms and structural changes.

System class	Temperature role	Dominant mechanism	Structural change
Biodegradable nanoparticles	Kinetic accelerator	Diffusion, degradation	Increased porosity, chain scission
LCST/UCST polymeric nanoparticles	Critical threshold	Polymer collapse, diffusion modulation	Coil-to-globule transition, dehydration
Thermo-sensitive liposomes	Critical threshold	Membrane permeability increase	Gel-to-liquid crystalline transition

doing so, this article is intended to serve both as a reference for researchers seeking to model temperature-dependent drug release and as a conceptual guide for the rational design of thermo-responsive delivery systems whose behavior can be predicted, optimized, and ultimately controlled through modelling.

2. Modelling frameworks for temperature-dependent drug release

A key milestone in this field was reached in 1961, when Professor Takeru Higuchi [71], a pioneering figure in physical pharmacy, introduced the Higuchi equation [72,73]. This model provided a simple yet rigorous description of drug release kinetics using semi-empirical principles and laid the theoretical foundation for the mathematical characterization of drug release from polymer-based dosage forms [73,74]. Since Higuchi's influential contribution, mathematical models for drug release have evolved from simple empirical equations to complex mechanistic descriptions capable of capturing multiple, simultaneous physicochemical processes. These models differ not only in their mathematical structure but, more importantly, in the depth of physical insight they provide into the underlying release mechanisms. While early empirical formulations were mainly developed to fit experimental data [75,76], later generations of models aimed to describe drug release using mass-balance principles, transport theory, polymer physics, and thermodynamics [77,78]. As a consequence, the modelling landscape today spans a broad variety: from purely descriptive relations, useful for rapid data interpretation, to fully mechanistic frameworks that explicitly include diffusion, degradation, swelling, erosion, dissolution, and interfacial phenomena [77,79].

In the context of temperature-dependent systems, this distinction becomes particularly important. Temperature does not simply accelerate diffusion or degradation; instead, it can induce abrupt structural transitions, such as matrix liquefaction [22,80], polymer–solvent phase separation [81–83], collapse of polymers [84,85], or melting of lipid bilayers [86,87]. These transitions fundamentally alter the transport pathways available to drug molecules. Therefore, incorporating temperature-dependency into drug release models requires a framework that can capture both smooth kinetics and discontinuous, switch-like transformations. To rationalize the wide variety of mathematical approaches proposed for the description of temperature-dependent drug release, it is useful to examine the construction and formulation of both empirical and mechanistic modelling approaches, focusing on how temperature is incorporated into drug release predictions. The development of an empirical model typically begins with the collection of experimental data under controlled conditions, such as drug release profiles measured at different temperatures or incubation times. These data are then processed using statistical or regression-based methods, often treated as a “black box,” in which the internal physicochemical mechanisms are not explicitly described. Instead, mathematical functions are fitted to the experimental outputs to capture observed patterns and dependencies. Once calibrated, empirical models can be used to interpolate or extrapolate trends within the experimental domain, offering rapid predictions with minimal computational effort. However, their predictive power is inherently limited to conditions similar to those

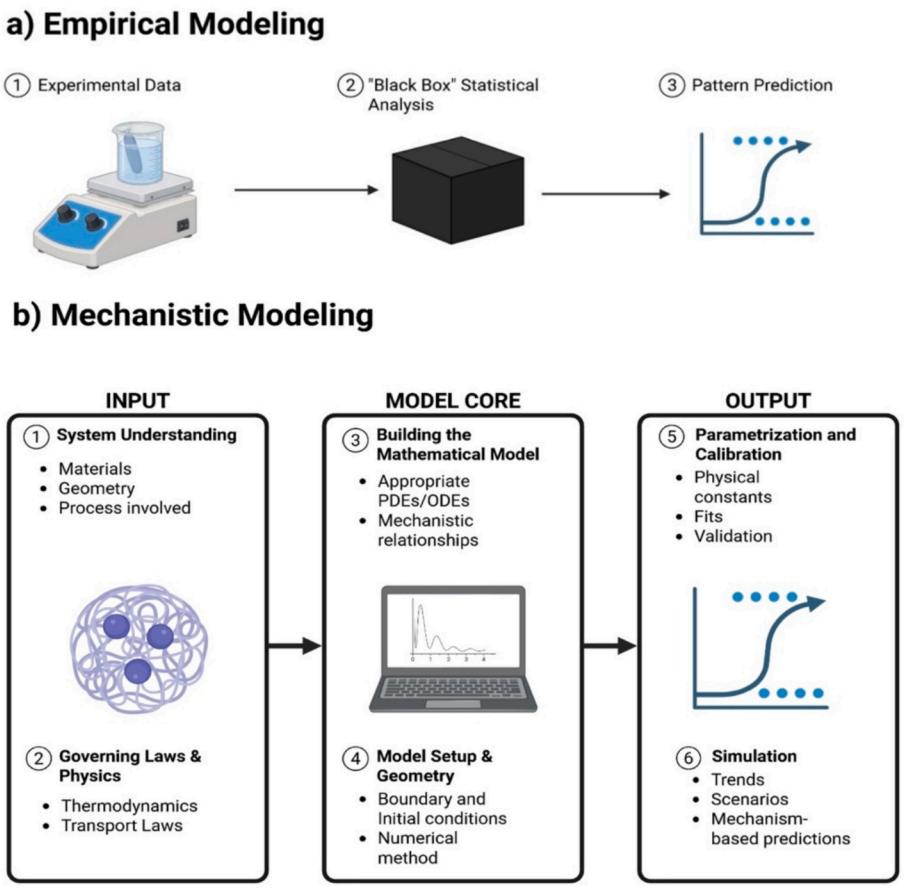

Fig. 3. Schematic representation of: a) Empirical modelling workflow. b) Mechanistic modelling workflow.

used for model fitting, and their parameters usually lack direct physical meaning. In contrast, mechanistic modelling is rooted in a fundamental understanding of the system and explicitly incorporates the governing physical and chemical principles that control drug release. The development of a mechanistic model begins with a detailed characterization of the system, including material properties, geometry, and the relevant transport or transformation processes. These features are then translated into governing laws, such as thermodynamic relationships, diffusion equations, or degradation kinetics.

Based on this understanding, an appropriate mathematical framework, often involving ordinary or partial differential equations, is constructed to describe the underlying mechanisms. Model setup further requires the definition of boundary and initial conditions, as well as the selection of suitable numerical methods for solution. Experimental data are subsequently used for parameterization and calibration, ensuring that model constants retain a clear physical interpretation. Once validated, mechanistic models enable simulation of different scenarios, exploration of parameter sensitivity, and mechanism-based predictions beyond the original experimental conditions. These models account for multiple coupled processes using fundamental balance equations and parameters with explicit physical and chemical meaning. This facilitates a direct connection between model variables and the intrinsic temperature-dependence of the drug carrier. Fig. 3 summarizes the steps needed for the development of both an empirical and a mechanistic model for the description of drug delivery from nanocarriers.

The following sections examine the main modelling strategies adopted in the literature for the description of the most common temperature-dependent systems for drug delivery. A summary is provided in Table 4.

2.1. *Biodegradable nanoparticles*

Biodegradable polymers have been extensively investigated as promising materials for drug encapsulation and delivery, attracting significant attention within the pharmaceutical industry [88–90]. This class of materials are characterized by low inflammatory potential, good permeability, and excellent therapeutic compatibility, making them highly suitable candidates for modern drug delivery applications [88]. Biodegradation is the process through which a polymer or material is progressively broken down into smaller, non-toxic molecules by biological and/or physicochemical mechanisms occurring under physiological conditions [91,92]. In drug delivery systems, this mechanism typically proceeds through hydrolysis of labile chemical bonds [93] (such as ester, carbonate, anhydride, or amide linkages) and/or enzymatic catalysis [94], ultimately producing biocompatible by-products that can be metabolized or excreted by the body [91,95]. Biodegradation alters the structural integrity, porosity, and mass of the carrier, thereby modulating drug release kinetics through simultaneous matrix erosion, chain scission, dissolution, and structural relaxation [96]. Biodegradable polymeric matrices represent a useful starting point for understanding temperature effects in drug delivery systems, both conceptually and mathematically. In such systems, drug release progressively increases with incubation temperature. From a kinetic point of view, this behavior is attributed to the fact that higher temperatures accelerate both enzymatic and non-enzymatic degradation processes, thereby enhancing matrix breakdown and facilitating drug diffusion [97]. PLGA nanoparticles are used in the section below as a representative example to illustrate the modelling strategy for systems in which drug release progressively increases with incubation temperature.

Their well-characterized temperature-dependent degradation and diffusion behavior makes PLGA an ideal model platform for outlining how thermal effects can be incorporated into mechanistic release models.

2.1.1. PLGA nanoparticles

Poly(lactic-*co*-glycolic acid) (PLGA) nanoparticles represent one of the most widely investigated biodegradable platforms for controlled drug delivery [80,98]. PLGA is a copolymer composed of lactic and glycolic acid monomers connected by hydrolytically labile ester bonds, which enable predictable degradation under physiological conditions [99]. When dispersed in aqueous media, PLGA chains aggregate into solid, spherical nanoparticles characterized by a compact hydrophobic polymer matrix which works as a reservoir capable of encapsulating a broad range of therapeutic agents, including hydrophobic drugs and, with appropriate formulation strategies, hydrophilic molecules [100]. To improve their biological performance, PLGA nanoparticles are frequently PEGylated, meaning that a layer of polyethylene glycol (PEG) chains is grafted or adsorbed onto their surface [101–103]. This PEG shell confers a hydrophilic corona that minimizes protein adsorption (opsonization) and reduces recognition by the mononuclear phagocyte system [104]. As a result, PEGylation significantly prolongs bloodstream circulation time, increasing the chances that the nanoparticles reach their intended biological target before being cleared [105]. Structurally, a PLGA nanoparticle behaves as a bulk-eroding polymeric matrix [106,107]. Water penetrates into the interior of the particle, initiating hydrolytic cleavage of ester linkages throughout the matrix rather than only at the surface [106,108,109]. Their degradation products, lactic and glycolic acid, are naturally metabolized via the Krebs cycle, ensuring excellent tolerability and safety [110]. This internal chain scission progressively reduces polymer molecular weight, increases porosity, and ultimately leads to mass loss and erosion.

As a consequence, PLGA nanoparticles can potentially exhibit multi-stage release behavior, typically characterized by an initial burst release, followed by a degradation–relaxation phase of the polymer matrix, and ultimately a diffusion-controlled (Fickian) stage [111,112]. However, this sequence is not universal. Depending on formulation parameters and degradation kinetics, PLGA systems may display mono-, bi-, or triphasic release profiles, reflecting different relative contributions of diffusion and polymer degradation mechanisms. As illustrated in Fig. 4, Type I corresponds to a monophasic release arising from a single homogeneous phase. Type II exhibits a biphasic behavior, characterized by an initial burst followed by a plateau-like, near zero-order release stage. In contrast, Type III displays a triphasic profile consisting of (i) an initial burst release, (ii) a subsequent diffusion-controlled phase, during which drug transport is governed by diffusion through a relatively dense polymer matrix with limited porosity, and (iii) a final accelerated stage dominated by polymer degradation, where chain scission, increased porosity, and matrix erosion markedly enhance drug mobility [113].

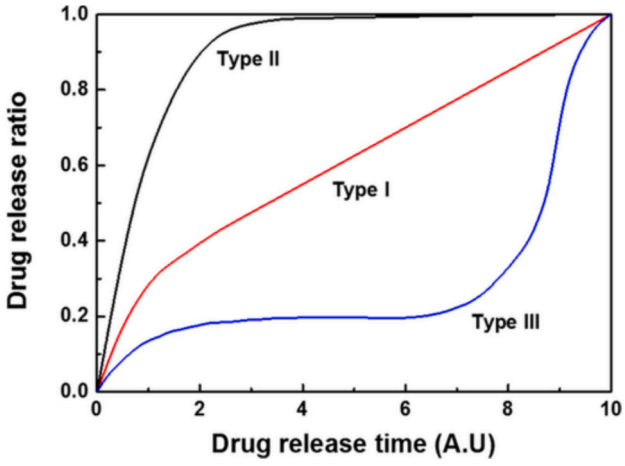

Fig. 4. Typical profiles of drug release including different release phases. Reprinted with permission from [113].

Although several mathematical models have been developed to describe these release behaviors, temperature is often neglected or treated as a constant parameter. Explicit incorporation of temperature-dependent effects can substantially enhance both the predictive capability and the mechanistic interpretability of these models. In this context, temperature may act either as a kinetic accelerator or as a variable capable of altering the dominant release mechanism, depending on the relative importance of polymer degradation. This dual role is particularly evident when comparing diffusion-dominated and degradation-driven PLGA systems. In the work of Sunazuka et al. [114], where polymer degradation is negligible over the experimental timescale, temperature primarily accelerates drug release without altering the overall shape of the release profile. The system exhibits a typical biphasic behavior, consisting of an initial burst followed by a diffusion-controlled phase. In this study drug release is described by the analytical solution of Fick's second law of diffusion for spherical systems, corrected to account for the initial burst contribution:

$$\frac{M_t}{M_\infty} = \left[1 - \frac{6}{\pi^2}\sum_{n=1}^{\infty}\frac{1}{n^2}\exp\left(-\frac{\pi^2 n^2 D t}{r^2}\right)\right]*(1-b)+b \tag{1}$$

where M_t and M_∞ are the mass of the drug released at time t and that at time approaching infinity, respectively, D is the drug diffusion coefficient, r is the radius of the sphere and $b = \frac{M_{burst}}{M_\infty}$ represents the fraction of drug released during the initial burst phase. In this approach, the effect of temperature was accurately captured through an Arrhenius-type dependence of the effective diffusion coefficient which shows the relationship among the drug diffusion constant (D), the absolute temperature (T), and the activation energy (Ea) at that temperature as shown in Eq. (2).

$$D = D_0\exp\left(-\frac{E_a}{RT}\right) \tag{2}$$

In contrast, the study by Shafiee et al. [115] demonstrates that when polymer degradation becomes significant, temperature fundamentally reshapes the release curve.

At low temperatures (4–25 °C), the system exhibits diffusion-dominated, biphasic release profiles similar to those observed in non-degrading nanoparticles. However, at higher temperatures (≥37 °C), the release profile transitions to a characteristic triphasic behavior, with a reduced initial burst, a shortened diffusion phase, and a markedly accelerated degradation-driven stage. This transition is associated with enhanced water uptake and a strong acceleration of hydrolytic degradation, as evidenced by the rapid decrease in polymer molecular weight. To capture this complex behavior, Shafiee et al. employed a multi-mechanistic model combining distinct release contributions:

$$f(t) = f_1\left(1-e^{-k_b t}\right) + f_2\left(1 - \frac{6}{\pi^2}\sum_{n=1}^{\infty}\frac{1}{n^2}\exp\left(-\frac{\pi^2 n^2 D t}{r^2}\right)\right) + f_3\left(\frac{e^{k_d t - k_d t_{max}}}{1+e^{k_d t - k_d t_{max}}}\right) + f_4\left(k_p t^{n_p}\right) \tag{3}$$

Here, $f(t)$ represents the cumulative fraction of drug released, while f_1, f_2, f_3, and f_4 denote the relative contributions of burst release, diffusion, degradation, and post-degradation transport, respectively, with their sum equal to unity. The parameters k_b, k_d, and k_p are kinetic constants associated with burst release, degradation, and the Peppas model, respectively; D is the effective diffusion coefficient, t_{max} is the characteristic time of the degradation phase, r is the system radius, and n_p is the diffusional exponent of the Peppas model. Unlike diffusion-controlled systems, where temperature dependence can be captured through a single Arrhenius relationship applied to the diffusion coefficient, this

multi-stage model requires several parameters, including diffusion coefficient (D), degradation kinetics constants (k_b, k_d, and k_p), and the characteristic time of degradation (t_{max}), to be treated as temperature dependent, each following a distinct Arrhenius behavior. This reflects the fact that, in degradation-driven systems, temperature does not merely accelerate release but also modifies the relative contribution of the underlying mechanisms, ultimately reshaping the release profile itself.

A similar approach has been demonstrated in the work of Lucero-Acuña et al. [112], where the three stages of the release profile are described as follows: the initial burst is represented by a first-order kinetic equation; the degradation–relaxation phase is captured through the Prout–Tompkins model; and the diffusion-controlled (Fickian) stage is evaluated using a general mass balance formulated in radial coordinates, owing to symmetry considerations. The governing equation obtained from coupling these three release mechanisms can be expressed as shown in Eq. (4).

$$\frac{M_t}{M_\infty} = \theta_b[1-\exp(-k_b t)] + \theta_r\left\{\frac{\exp[k_r(t-t_{max})]}{1+\exp[k_r(t-t_{max})]}\right\} + \theta_d\left[1-\frac{6}{\pi^2}\sum_{n=1}^{\infty}\frac{1}{n^2}\exp\left(-\frac{\pi^2 n^2 D_e t}{r^2}\right)\right] \quad (4)$$

where M(t)/M∞ represents the drug fraction released, t is the release time, θ_b, θ_r, and θ_r are the contribution fractions of initial burst, nanoparticle degradation–relaxation, and diffusion mechanisms, respectively, over the total mass drug release. The effect of temperature on the initial burst constant (k_b), the degradation–relaxation rate constant (k_r), the time required to reach 50% drug release (t_{max}), and the effective diffusion coefficient (D_e) were evaluated using equations based on the Arrhenius model. For all the models described above, parameter estimation can be performed by fitting the model to experimental release data collected at a minimum of three different temperatures, using a nonlinear least-squares algorithm implemented in MATLAB® (MathWorks, USA), thereby ensuring reliable identification of temperature-dependent parameters.

2.2. Thermo-responsive polymeric systems (LCST/UCST)

When discussing thermo-responsiveness in polymeric nanoparticles for drug delivery, polymers exhibiting Lower Critical Solution Temperature (LCST) or Upper Critical Solution Temperature (UCST) behavior are of primary interest [116].

LCST polymers become insoluble in water above a specific critical temperature, while UCST polymers become insoluble below a certain critical temperature [117–119]. Among LCST systems, poly(N-isopropylacrylamide) (PNIPAM) is the most extensively investigated and widely recognized prototype for drug delivery applications, thanks to its coil-to-globule transition in aqueous media at approximately 32 °C, a temperature close to physiological conditions [120–123]. Below its LCST, PNIPAM chains remain hydrated and expanded as a result of favorable hydrogen-bonding interactions with surrounding water molecules [124,125]. When the temperature exceeds the LCST, these interactions weaken, leading to dehydration of the polymer chains, collapse into a compact globular state, increased hydrophobicity, and reduced polymer–solvent affinity [19,126]. This abrupt conformational transition has important consequences for controlled drug delivery. As polymer solubility decreases, the chains reorganize to minimize contact with the aqueous environment, often resulting in particle shrinkage, chain aggregation, or structural collapse of the carrier matrix [84]. Such temperature-induced rearrangements can destabilize drug–polymer interactions, expel water from the network, and shorten diffusion pathways, thereby promoting the release of encapsulated payloads [127]. Recent literature further demonstrates the rapid development of thermo-responsive intelligent drug-delivery carriers incorporating PNIPAM, moving beyond conventional single-function polymeric systems. For example, hybrid PNIPAM-based microgel platforms have been engineered to couple thermal responsiveness with disease-specific functional performance, such as modulation of aqueous lubrication in osteoarthritis-related nanocarriers [122]. Likewise, multifunctional systems based on PEG-g-PNIPAM-coated nanoMOFs or core–shell nanoMOFs@microgel have shown that thermo-responsive swelling/collapse can be integrated with controlled drug release and additional therapeutic functions, including anti-inflammatory activity [124,125]. In the oncology field, magnetic cellulose-grafted P(NIPAM-co-DMAEA) nanocarriers have further illustrated how LCST-triggered release can be combined with pH sensitivity and magnetic targeting, enabling enhanced cisplatin release under acidic and mildly hyperthermic conditions [123].

These studies highlight a clear trend toward advanced hybrid nanocarriers in which thermo-responsiveness is embedded within multifunctional, intelligent delivery platforms rather than treated as an isolated material property. Beyond PNIPAM, several other LCST polymers have been explored to broaden the design space of thermo-responsive nanocarriers. Poly(oligo(ethylene glycol) methacrylate) (POEGMA) and related OEG-based methacrylates are particularly attractive because their LCST can be finely tuned over a broad range (≈26–90 °C) by adjusting side-chain length, copolymer composition, and hydrophilic–lipophilic balance, while also showing improved biocompatibility and reduced thermal hysteresis compared with PNIPAM [38,128,129]. This compositional tunability makes POEGMA derivatives especially suitable for designing systems that respond close to mild hyperthermia or physiological temperature. Another relevant LCST polymer is poly(N-vinylcaprolactam) (PNVCL), a non-ionic and water-soluble material often considered a biocompatible alternative to PNIPAM [130]. Its phase-transition temperature can be modulated through copolymerization with hydrophilic or ionic monomers, allowing responsive behavior across a wide temperature window [131,132]. Owing to its low toxicity and reversible collapse in aqueous media, PNVCL has been widely investigated for smart micelles, nanogels, and drug carriers [133,134]. The typical reported release behavior for LCST-triggered nanocarriers is a biphasic profile consisting of an initial rapid burst, followed by a slower sustained stage governed by diffusion of molecules entrapped deeper within the collapsed carrier structure [40,135]. The incorporation of thermo-responsive behavior into mathematical models remains particularly challenging because drug release is often not a smooth or gradual function of temperature. Rather, the transition frequently occurs over a relatively narrow thermal window around the critical solution temperature, where abrupt changes in polymer hydration, chain conformation, and carrier permeability can produce switch-like variations in release kinetics. Capturing this discontinuous behavior requires specific modelling strategies, which can be implemented using different mathematical formulations depending on the complexity and physical assumptions of the model.

2.2.1. Empirical and semi-empirical models

These approaches describe drug release as a function of time using equations that contain empirical parameters [76]. To incorporate thermo-responsiveness into such models, a common strategy is to evaluate how these empirical parameters change with temperature. In the study by Ribeiro et al. [136], drug release from an LCST-based system consisting of folic-acid-functionalized PNIPAM-co-PEGMA-co-allylamine crosslinked nanoparticles (FANPs) was analyzed by fitting the experimental DOX release profiles at 37 °C and 40 °C to two classical empirical models: the Higuchi model [137] and Korsmeyer–Peppas [138,139]. The mathematical expressions for the two models are presented in Eq. (5) and (6), respectively.

$$\frac{M_t}{M_\infty} = \sqrt{\frac{2C_0 D\varepsilon t}{\tau\pi}} = K_H\sqrt{t} \quad (5)$$

This equation is specifically applicable to porous matrices that are initially saturated with the drug. Where M(t)/M∞ represents the drug fraction released, t is the release time, C_0 is the concentration of the diffusing drug in the porous matrix, D is the diffusivity in the matrix medium, ε is the porosity of the matrix and τ is its tortuosity factor. On the right-hand side of the equation, all terms related to concentration, diffusion, tortuosity, and porosity are assumed to be constant and are grouped into a single parameter, K_H, known as the Higuchi constant.

$$\frac{M_t}{M_\infty} = Kt^n \tag{6}$$

Where n is the time exponent indicative of the drug release mechanism as explained in Table 2, and K is a constant that depends on the shape and geometric characteristics of the drug carrier vesicle or matrix.

The empirical parameter values, below/near and above the LCST, obtained by Ribeiro and coworkers are reported in Table 3.

The use of only two temperature points (37 and 40 °C) does not permit reconstruction of the full continuous LCST transition. However, it still offers a comparative snapshot of carrier behavior under two relevant thermal states: below/near and above the responsive region. Despite this simplification, the comparison remains mechanistically informative because it captures how release behavior changes across temperatures in the vicinity of the LCST, where the most pronounced structural variations are expected to occur. Together, the temperature-dependent evolution of K_H, K, and n provides a coherent quantitative picture of LCST-triggered behavior. In particular, the marked increase in K_H and K, coupled with a decrease in n above the LCST, reflects the switch-like nature of thermo-responsive diffusion: transport becomes faster overall, yet increasingly constrained within a collapsed polymer network. This combination of trends is consistent with diffusion remaining the dominant release mechanism, though under non-ideal conditions.

In fact, values of the release exponent below the theoretical Fickian limit for spherical systems ($n \approx 0.43$) are frequently reported in the literature and are generally interpreted as indicative of diffusion-controlled, but hindered, transport. For example, Hahn et al. [151] reported n values as low as 0.38 in nanoparticle–polymer composites and attributed them to Fickian diffusion occurring under retarded conditions rather than to a different mechanism. Similarly, Pu et al. [152] described $n < 0.43$ as characteristic of pseudo-Fickian behavior, reflecting constrained or slowed diffusion rather than the absence of diffusion-driven release. In thermo-responsive systems, this deviation has a well-defined physical origin: above the LCST, the polymer undergoes a coil-to-globule transition, resulting in a collapsed, less hydrated, and structurally heterogeneous network [127,153,154]. This conformational change leads to a reduction in free volume and an increase in tortuosity of the diffusion pathways, all of which contribute to hindered mass transport [153]. Consequently, diffusion remains the prevailing release mechanism, but proceeds under increasingly constrained conditions, as reflected by the lower n values. Overall, these observations highlight that LCST polymers naturally exhibit switch-like, diffusion-dominated release profiles, and that classical kinetic models, when interpreted with appropriate physical insight, can effectively capture the mechanistic impact of thermally induced structural transitions. According to this modelling strategy, the temperature-dependent behavior of the empirical parameters in these models can be represented as a step function,

Table 2
Release exponent n of the Peppas equation and drug release mechanism from polymeric controlled delivery systems of different geometry [52].

Thin film	Exponent, n		Drug release mechanism
	Cylinder Sphere		
0.5	0.45	0.43	Fickian diffusion
$0.5 < n < 1.0$	$0.45 < n < 0.89$	$0.43 < n < 0.85$	Anomalous transport
1.0	0.89	0.85	Polymer swelling

Table 3
Fitting of the FANPs drug release kinetic models.

Temperature	Higuchi		Korsmeyer-Peppas		
	R^2	K_H	R^2	K	n
37 °C	0.8580	7.47	0.9482	14.45	0.324
40 °C	0.6737	11.96	0.9438	30.28	0.251

treating the regions below and above the critical temperature as distinct regimes. The Higuchi constant, shown in Eq. (7), can be taken as a representative example.

$$K_H(T) = \begin{cases} K_{H\ swollen}, & T < T_{LCST} \\ K_{H\ collapsed}, & T \geq T_{LCST} \end{cases} \tag{7}$$

While mathematically convenient, the step-function representation should be interpreted only as an idealized first-order approximation. The LCST transition is not a true mathematical discontinuity; rather, it occurs over a finite temperature interval that depends on copolymer composition, concentration and environmental conditions, within which polymer hydration, conformation, and permeability change rapidly.

As a result, the system may exhibit an apparently switch-like response in the vicinity of the transition temperature. Although a step function can be useful as a simplified limiting case, a sigmoidal expression generally provides a more realistic mathematical description, as it captures the continuous yet steep variation of the release-related parameters across the LCST region [155]. A possible sigmoidal representation is given in Eq. (8) for the Higuchi constant.

$$K_H(T) = K_{H\ swollen} + \frac{K_{H\ collapsed} - K_{H\ swollen}}{1 + e^{-k(T - T_{LCST})}} \tag{8}$$

Where $K_{H,\text{collapsed}}$ and $K_{H,\text{swollen}}$ are the Higuchi constants corresponding to the nanoparticle state above and below the LCST respectively, the parameter k governs the sharpness of the temperature-induced transition in the Higuchi constant. It can be regarded as a phenomenological descriptor of the cooperativity of the LCST response. Specifically, larger k values correspond to a steeper and narrower transition region, consistent with a more cooperative coil-to-globule collapse and a more abrupt change in polymer hydration, permeability, and transport properties. In contrast, smaller k values indicate a broader transition interval, which may reflect reduced cooperativity or increased heterogeneity in polymer composition, crosslinking density, or local microenvironment. From a thermodynamic perspective, k can therefore be viewed as an empirical indicator of how sharply polymer–solvent compatibility changes with temperature in the LCST region, that is, how rapidly the system evolves from the hydrated, swollen state to the collapsed, poorly solvated state. While demonstrated here for the Higuchi constant, the proposed sigmoidal framework can be extended to most empirical and semi-empirical release models by expressing their temperature-dependent parameters as continuous functions across the LCST region. Importantly, this allows each fitted parameter to serve as an indirect indicator of the physicochemical processes underlying the LCST transition, including changes in polymer–solvent compatibility, hydration, structural collapse, and transport resistance.

2.2.2. Mechanistic models

However, when developing mechanistic models, this is not enough. Mechanistic models are constructed from fundamental principles, incorporating all relevant transport and physicochemical mechanisms. When the temperature crosses the LCST or UCST, the polymer matrix undergoes a conformational collapse, resulting in a denser shell structure and reduced permeability. In addition to this, once the transition temperature is crossed, the polymer becomes more hydrophobic and collapses, reducing water content and shortening the diffusional path length within the nanoparticle. Collectively, these structural changes result in a faster drug transport toward the surrounding medium. For

Table 4
Drug release models summarized description.

Model	Principle & Description	Advantages	Limitations	Reference
Empirical / semi-empirical release models (Higuchi; Korsmeyer–Peppas)	Drug release described by analytical expressions fitted to experimental data; temperature-dependence incorporated indirectly through temperature-dependent fitting parameters	Simple implementation; low computational cost; useful for rapid comparison of release profiles at different temperatures	No mechanistic background; parameters lack direct physical meaning;	[73,139]
Arrhenius-type kinetic models	Temperature dependence introduced through Arrhenius expressions for degradation and diffusion rate constants	Physically intuitive; suitable for biodegradable systems where temperature accelerates kinetics	Inadequate for more complex and irregular temperature-dependence behavior	[112]
Flory–Huggins thermodynamic framework	Polymer–solvent miscibility governed by $\chi FH(T,\phi)$; predicts LCST/UCST and phase separation	Physically grounded; directly links temperature to solubility and phase behavior	Requires extensive phase-behavior data and complex fitting procedures	[82,140,141]
Core–shell diffusion models	Drug transport described by coupled diffusion–reaction equations in spherical core–shell geometry	Explicit coupling between structure, geometry, and transport	Requires detailed geometric data; increased mathematical complexity	[142]
Thermo-sensitive liposome models	Heat transfer governs bilayer melting, defining lag time and ON/OFF permeability	Captures phase-transition-triggered release and lag time	Assumes a single sharp Tm; neglects sub-transition leakage	[143]

Table 5
Experimental techniques for proper parameter estimation.

Parameter	Physical meaning	Role in temperature-dependent modelling	Experimental technique (s)	Notes	Reference
Nanoparticle size and morphology	Temperature-dependent particle dimension (hydrodynamic or physical radius)	Directly affects diffusion length, surface-to-volume ratio, and geometry in diffusion and core–shell models	DLS, TEM, cryo-TEM	DLS provides R(T) in hydrated conditions; microscopy validates morphology and core–shell structure	[127,144,145]
Cloud-point temperature Tcp (ϕ)	Temperature at which phase separation begins at a given concentration	Identifies critical transition region for thermo-responsive behavior	UV–Vis turbidimetry, DLS	Tcp definition must be stated (onset, inflection, or fixed transmittance criterion)	[81,146]
Flory–Huggins interaction parameter χ_{FH} (T,ϕ)	Thermodynamic indicator of polymer–solvent compatibility	Links temperature to solubility, phase behavior, and structural transitions	Indirectly obtained from cloud-point data and binodal fitting	χ_{FH} reconstructed by enforcing equality of chemical potentials	[82,140]
Effective drug diffusion parameters	Drug transport rates within carrier	Control temperature-dependent release kinetics	Drug-release experiments coupled with UV–Vis or HPLC quantification	Extracted by fitting release profiles at different temperatures	[142,147,148]
Drug solubility C_s(T)	Saturation concentration of drug in release medium	Enters diffusion–dissolution and solubility-limited models	UV–Vis spectroscopy, HPLC	Determined under equilibrium conditions at controlled temperature	[149]
Thermal transition temperatures	Characteristic temperatures of phase or conformational transitions	Define sharp transition behavior in thermo-responsive systems	DSC (polymers and lipids)	DSC provides transition temperature and transition sharpness	[150]

this reason, when modelling these types of thermo-responsive drug delivery systems, it is essential to introduce a relationship between temperature and nanoparticle size. This relationship originates from the reduction in polymer solubility once the critical temperature is reached, which drives polymer chain collapse, particle shrinkage, or aggregation. The modelling strategy can be outlined as shown in Fig. 5: first, describe the dependence of solubility on temperature; then, relate solubility to nanoparticle size.

2.2.2.1. Step 1: solubility and temperature (Flory-Huggins theory). From a thermodynamic perspective, in LCST-type polymers, dissolution in the external medium is energetically favorable below the transition temperature because the Gibbs free energy of mixing is negative [156]. This is primarily due to favorable enthalpic contributions from hydrogen bonding and a relatively low entropy of mixing. However, as the temperature rises above the LCST, hydrogen bonds between the polymer and water molecules are disrupted, and bound water is released. This results in an increase in the enthalpy contribution, while the entropy term decreases due to the released water molecules [157]. The combined effect of these changes causes Gibbs free energy of mixing to become positive, driving the polymer from a soluble to an insoluble state. The Gibbs free energy of mixing for a polymer–solvent system can be described using Flory–Huggins theory [158,159], as shown in Eq. (9).

$$\Delta G = \Delta H - T\Delta S = RT\left(\frac{\varphi_1}{N_1}\ln\varphi_1 + \frac{\varphi_2}{N_2}\ln\varphi_2 + \chi_{FH}\varphi_1\varphi_2\right) \quad (9)$$

Where ΔG is the free energy of mixing per unit volume, ΔH is enthalpy of mixing per unit volume, ΔS is the combinatorial entropy per unit of volume, R is the gas constant, T is the absolute temperature, φ_1 and φ_2 and N_1 and N_2 are the volume fractions and relative molar volumes of component 1 (solvent) and component 2 (polymer) respectively, and χ_{FH} is the Flory-Huggins interaction parameter. Within this framework, the enthalpic contribution, is proportional to the Flory–Huggins interaction parameter (χ_{FH}) and the product of solvent (φ_1) and polymer

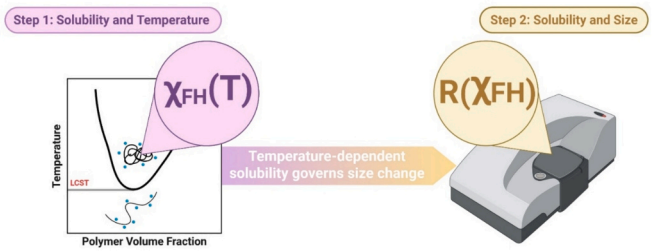

Fig. 5. Two-step modelling strategy.

(φ_2) volume fractions. When χ_{FH} is low, polymer–solvent interactions are sufficiently favorable to compensate the entropy loss associated with mixing long polymer chains, resulting in a negative Gibbs free energy of mixing and complete miscibility. In opposition, when χ_{FH} rises above a critical value, the free energy becomes positive, promoting phase separation and reduced polymer solubility. Quantitatively, values of χ_{FH} significantly greater than 0.5 are generally indicative of nonsolvency [160].

For this reason, χ_{FH} is widely employed as a thermodynamic indicator of polymer–solvent compatibility and as a fundamental parameter for constructing phase diagrams, including binodal and spinodal curves [161]. A widely adopted and computationally convenient formulation of the Flory–Huggins interaction parameter (χ_{FH}) expresses it as the product of a temperature-dependent factor, D(T), and a concentration-dependent factor, B(φ_2), such that:

$$\chi_{FH}(T,\varphi_2) = D(T)B(\varphi_2) \tag{10}$$

Where, according to the work by C. Qian et at. [140] the two factors can be expressed as shown in Eq. (11) and (12).

$$D(T) = d_0 + \frac{d_1}{T} \tag{11}$$

$$B(\varphi_2) = 1 + b_1\varphi_2 + b_2\varphi_2^2 \tag{12}$$

It is important to note that, to accurately describe LCST behavior, $d_1 < 0$, whereas for UCST behavior, $d_1 > 0$. The coefficients b_i and d_i can be determined through a fitting procedure of experimental data of critical solution temperatures and polymer concentrations along the liquid–liquid coexistence curve (or binodal curve). The expression adopted here represents only one possible temperature- and composition-dependent form of the Flory–Huggins interaction parameter. Across the thermodynamics literature, many alternative χ_{FH} formulations have been proposed to address the limitations of the classical model. As highlighted by Chang and Bae [162], accurate descriptions of LCST behavior require explicitly accounting for strong, directional specific interactions, particularly hydrogen bonding, whose temperature dependence cannot be captured by the simple $\chi_{FH} \propto 1/T$ relation. Jung and Bae [82] extended this approach by introducing a specific-interaction parameter based on oriented segment–segment contacts, showing that such improved models can reproduce LCST, closed-loop miscibility, and other complex phase behaviors inaccessible to the classical theory.

Knowing that, at a given temperature, the liquid-liquid coexistence curve, or binodal curve, intersects at two points which represent the compositions of the coexisting equilibrium phases, the fitting procedure can be carried out by imposing the equality of the polymer's chemical potential in the polymer-rich and polymer-poor phases and by consequently determining the corresponding parameters of the interaction parameter expression.

$$\Delta\mu_i = \left(\frac{\partial \Delta G}{\partial n_i}\right)_{T,P,n_j} \tag{13}$$

$$\Delta\mu_1' = \Delta\mu_1'' \tag{14}$$

$$\Delta\mu_2' = \Delta\mu_2'' \tag{15}$$

Where the prime and double prime denote two different phases. Eq. (14) and (15) must be solved simultaneously to obtain the binodal curve. This approach allows the parameters of the χ_{FH} expression to be determined consistently with phase equilibrium data. In particular, allowing for the successive development of the complete phase diagram as shown in Fig. 6: spinodal curve and critical point can be identified according to Eq. (16) and (17).

$$SPINODAL: \left(\frac{\partial^2 \Delta G}{\partial \varphi_2^2}\right)_{T,P} = 0 \tag{16}$$

$$CRITICAL\ POINT: \left(\frac{\partial^2 \Delta G}{\partial \varphi_2^2}\right)_{T,P} = \left(\frac{\partial^3 \Delta G}{\partial \varphi_2^3}\right)_{T,P} = 0 \tag{17}$$

Once the phase diagram is complete with binodal curve (found experimentally), spinodal curve and critical point, the dependency of solubility on temperature is clear. It is now important to proceed by linking solubility to nanoparticle size.

2.2.2.2. Step 2: solubility and size. In the model developed by Cowen et al. [141], the Flory–Huggins interaction parameter is directly linked to nanoparticle dimensions, establishing a quantitative connection between solubility and particle size. This study demonstrated that nanoparticle formation is controlled by the relative position of χ_{FH} with respect to the spinodal boundary for phase separation. To quantify this, they introduced the parameter $\chi_{Spinodal}$ shown in Eq. (18).

$$\Delta\chi_{Spinodal} = \chi_{FH} - \chi_{Spinodal} \tag{18}$$

Where $\chi_{Spinodal}$ represents the minimum χ_{FH} required for spontaneous phase separation, at a given composition, through spinodal decomposition and it can be evaluated once the whole phase diagram is known. Within this regime characterized by $\Delta\chi_{Spinodal} > 0$, Cowen et al. observed a linear relationship between the hydrodynamic diameter (D) and $\Delta\chi_{Spinodal}$. This correlation was established by measuring the

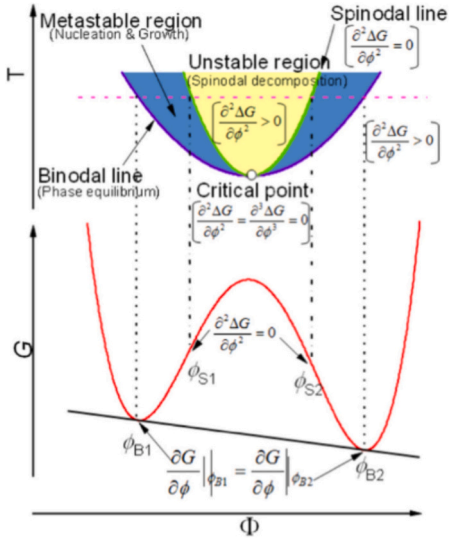

Fig. 6. Binodal and spinodal phase diagram and the corresponding Gibbs free energy curve of a binary mixture with a lower critical solution temperature (LCST). Reprinted with permission from [81].

hydrodynamic diameter of the synthesized nanoparticles using Dynamic Light Scattering (DLS). At each composition, the corresponding Flory–Huggins interaction parameter was calculated using the previously derived expression.

Then, by plotting the hydrodynamic diameter against the calculated χ_{FH} and consequently the $\Delta\chi_{Spinodal}$ values, the relationship between nanoparticle size and polymer–solvent interaction parameter was determined. This method can be repeated at different temperatures. However, it is important to note that the condition $\Delta\chi_{Spinodal} > 0$ does not necessarily imply immediate or purely spontaneous demixing in real polymer systems. While this condition defines the thermodynamic instability of the homogeneous phase, the actual evolution of phase separation is strongly influenced by kinetic factors such as polymer chain mobility, solution viscosity, degree of entanglement, and the rate at which the system is driven into the unstable region [163,164]. As a result, the development of concentration fluctuations and the resulting morphology may deviate significantly from ideal spinodal behavior, particularly in polymer systems where diffusion is intrinsically slow and constrained by chain connectivity and entanglement effects [165]. In light of this, it is important to emphasize that the observed linear relationship between $\Delta\chi_{Spinodal}$ and nanoparticle diameter should not be interpreted as a universal thermodynamic law [166]. While $\Delta\chi_{Spinodal}$ represents the thermodynamic driving force for phase separation, the final particle size is the result of a complex interplay between thermodynamics and kinetics [164]. In particular, $\Delta\chi_{Spinodal}$ controls the depth of the system within the unstable region and therefore influences the rate of growth of concentration fluctuations and the characteristic length scale associated with spinodal decomposition [167]. However, the ultimate nanoparticle size depends on kinetic factors such as diffusion rates, coarsening dynamics, and the possible arrest of phase separation [163]. As a result, this linear trend should be interpreted as an empirical relationship that holds only under specific conditions: within a limited range of polymer fraction and for systems undergoing spinodal-type phase separation [141]. Indeed, when working below the spinodal threshold ($\Delta\chi_{Spinodal} < 0$), phase separation does not proceed spontaneously, as the system lies in a metastable regime where a free-energy barrier must be overcome.

In this region, phase separation can only occur if two conditions are satisfied: (i) the system is thermodynamically driven toward demixing, i.e., it lies above the binodal boundary ($\Delta\chi_{Binodal} > 0$), and (ii) a kinetic pathway is available to overcome the nucleation barrier, for instance through the presence of suitable nucleation sites As a result, phase separation in this regime follows a nucleation-and-growth mechanism, in contrast to the barrierless spinodal decomposition observed when $\Delta\chi_{Spinodal} > 0$ [167]. This implies that phase separation requires overcoming a free-energy barrier for the formation of stable nuclei, making the resulting morphology highly sensitive to processing conditions such as heterogeneities, nucleation sites, and external perturbations. In addition, factors such as finite quench rates and mass transport limitations can significantly affect both nucleation density and subsequent growth dynamics [163,166]. Although both regimes are governed by an interplay between thermodynamics and kinetics, spinodal decomposition leads to the formation of concentration fluctuations with a well-defined characteristic size, corresponding to the typical spatial scale of the emerging polymer-rich and polymer-poor domains [164]. This length scale is directly influenced by the thermodynamic driving force and, if phase separation is kinetically arrested at an early stage, it can be preserved and reflected in the final nanoparticle size. By contrast, nucleation-and-growth processes do not exhibit a predefined structural length scale, as particle size results from stochastic nucleation events and subsequent growth dynamics, and is therefore strongly dependent on processing conditions rather than uniquely controlled by $\Delta\chi_{Binodal}$ [168]. As a result, while $\Delta\chi_{Spinodal}$ may lead to a clear linear correlation with nanoparticle size in systems undergoing spinodal decomposition (i.e., in the absence of a nucleation barrier), the equivalent $\Delta\chi_{Binodal}$ cannot provide a reliable relationship. In practice, many polymer systems exhibit behavior that lies between ideal spinodal decomposition and classical nucleation-and-growth regimes, forming a continuum rather than two sharply separated mechanisms [164]. In particular, kinetic arrest phenomena may prevent the system from reaching its equilibrium phase-separated state.

Increasing viscosity, reduced diffusion rates, chain entanglement, or vitrification-like transitions can effectively "freeze" the evolving morphology at early stages of phase separation [165,168]. Under these conditions, the final nanoparticle size reflects the transient characteristic length scale of concentration fluctuations rather than equilibrium thermodynamic predictions. Taken together, these considerations suggest that the relationship between thermodynamic driving forces and nanoparticle size must account for the specific kinetic pathway followed during phase separation. In addition to this, the nanoparticle size obtained from DLS and used in the present framework represents a hydrodynamic diameter rather than a purely geometric quantity [144,169]. In thermo-responsive polymer systems, this effective size includes contributions from both the polymer structure and its surrounding hydration shell and is therefore strongly influenced by temperature-dependent polymer–solvent interactions [170]. As a consequence, the measured size reflects different physical states of the system: a swollen and highly hydrated configuration below the LCST, and a collapsed, less solvated structure above it. In the vicinity of the LCST, where the transition occurs over a finite temperature range, DLS measurements may further represent an apparent or averaged dynamic structure, potentially influenced by coexistence of partially collapsed and swollen domains, as well as by transient aggregation phenomena [127,171]. Consequently, variations in particle size with temperature should not be interpreted solely as geometric expansion or contraction, but rather as the combined result of structural rearrangement, dehydration, and changes in polymer chain conformation [172]. This distinction is particularly relevant when coupling nanoparticle size to thermodynamic parameters such as χ_{FH}, since the resulting size reflects an effective, transport-relevant dimension rather than a fixed physical boundary. In this context, the hydrodynamic diameter should be interpreted as the characteristic length scale governing mass transport, implicitly incorporating both structural and solvation effects. Taken together, these considerations highlight that temperature-induced variations in solubility and nanoparticle size are deeply interconnected.

A decrease in χ_{FH} enhances polymer–solvent affinity, promoting swelling and increasing the effective particle radius, whereas an increase in χ_{FH} has the opposite effect, favoring polymer collapse and shortening the diffusion pathways within the carrier. Because solubility and geometry are tightly coupled, any realistic description of drug release must treat these quantities not as fixed constants, but as dynamic, temperature-dependent properties that shape the internal mass-transport phenomena of the nanoparticle. A natural way to incorporate this physicochemical knowledge into a mechanistic framework is through continuum-scale models that explicitly account for nanoparticle geometry. A particularly illustrative example is the two-layer core–shell model developed by Pontrelli et al. [142]. In their formulation, the nanocarrier is represented as a spherical structure composed of a drug-loaded core surrounded by a responsive polymeric shell. Drug transport is described through coupled nonlinear partial differential equations for dissolution and diffusion in the core, and diffusion–reaction kinetics in the shell, while the geometry is defined by the inner and outer radii (R_0 and R_1) and it enters directly into the governing equations and boundary conditions. As a result, changes in nanoparticle size or shell thickness have an immediate and quantifiable impact on the release behavior: a larger core increases the diffusion distance; a thicker shell enhances the barrier effect; and differences in volume fractions modulate the relative contributions of dissolution, diffusion, and drug retention. This explicit coupling between structure and transport makes the Pontrelli model especially valuable for thermo-responsive systems. Once $\chi_{FH}(T)$-driven variations in polymer–solvent affinity are known, the resulting changes

in solubility and nanoparticle size can be naturally introduced into the geometric and kinetic parameters of the model. In this way, the thermodynamic principles discussed in the previous section find a direct mathematical expression, enabling the model to capture how temperature simultaneously influences particle morphology and drug mobility. Extending such a framework to thermo-responsive nanocarriers therefore represents a promising route toward more predictive release models capable of describing the switch-like behavior characteristic of LCST and UCST polymers.

2.3. Thermo-sensitive liposomes (TSLs)

Liposomes are spherical vesicles formed by membrane bilayer composed by phospholipids surrounding an aqueous core [104]. This unique structure allows for the encapsulation of both hydrophilic and lipophilic drugs: hydrophilic compounds are entrapped within the aqueous interior, while lipophilic molecules are incorporated into the lipid membrane [173,174]. In the case of thermo-sensitive liposomes (TSLs), drug release occurs at the phase transition temperature (T_m) of the lipid bilayer [175,176]. At this temperature, the lipids transition from a solid gel phase to a liquid-crystalline phase, leading to a significant increase in membrane fluidity. The bilayer becomes more permeable to water and drugs in the liquid-crystalline state than in the gel phase [177,178]. The solid–liquid phase transition of the liposomal membrane offers an exceptional opportunity for achieving intelligent, temperature-triggered drug release. Similar to what has been described for LCST and UCST polymer systems, Fig. 7 shows how thermo-sensitive liposomes exhibit an "ON/OFF" release mechanism around their phase transition temperature (T_m). Below T_m, the membrane is in the gel phase and exhibits low permeability, while above T_m, the transition to the liquid-crystalline phase greatly enhances drug diffusion.

The main challenge in the mathematical modelling of such systems lies in accurately incorporating this discontinuous "ON/OFF" behavior into the model, ensuring that the abrupt change in permeability and release rate across the transition temperature is properly represented. The work of Mohammad Sirousazar [143] provides a solid foundation for the mathematical description of the phase-transition behavior of the phospholipid bilayer. This system is modelled as a spherical drug delivery platform consisting of three concentric layers: an inner drug core, an intermediate phospholipid bilayer shell and an outer protective polymeric shell. The outer polymeric shell (e.g., PEG [179,180], polydopamine [181]) is assembled on the liposomal surface to enhance colloidal stability, control drug release, and introduce stimuli-responsiveness, giving rise to so-called polymer-modified or polymer-caged liposomes [182,183]. In this model, the system is assumed to be in thermodynamic equilibrium with the release medium prior to the onset of operation ($t = 0$). Under these conditions, the bilayer shell is entirely in the solid phase, preventing drug diffusion; the system is therefore considered to be in its "OFF" state. When the temperature is suddenly increased above the phase transition temperature (T_m) at $t = 0$, the shell begins to gradually liquefy as heat is transferred from the surrounding medium to the liposome. During this process, a two-phase region, comprising both solid and liquid-crystalline domains, forms within the shell. Although the system is thermally activated and technically in its "ON" state, no drug release occurs until the shell is fully liquefied, at a time specified as t_{lag}. For times longer than t_{lag}, the drug molecules can dissolve within the liquefied shell and subsequently diffuse into the surrounding release medium. The mathematical modelling of the described drug delivery system in the ON state was carried out by solving the governing heat and mass transfer equations under pseudo-steady-state conditions, together with the appropriate boundary conditions for each layer. Thermo-responsiveness is introduced indirectly in this model: the temperature field obtained from the heat transfer equations enables the calculation of the melting-front position $R(t)$, the corresponding lag time t_{lag} required for complete liquefaction of the intermediate shell and the moment at which drug diffusion can effectively begin.

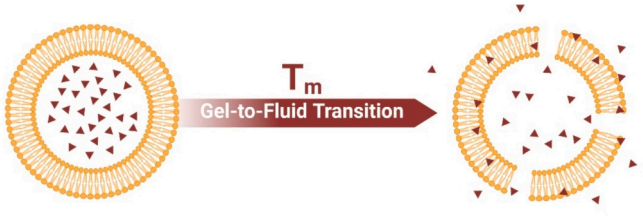

Fig. 7. Drug release at the phase transition temperature (Tm).

Basically, heat transfer determines both the geometry and the boundary conditions of the following mass-transfer problem, since the diffusion equations become applicable only once the entire shell has reached the phase transition temperature T_m. Therefore, the heat-transfer solution provides the temporal and spatial framework governing the onset and rate of drug release in the ON state and thus represents a prerequisite for any accurate modelling of thermo-responsive systems. Subsequently, solving the mass transfer equations allows for the definition of an expression for the cumulative amount of drug released in the ON state from the time t_{lag} to any given time t:

$$M_t = \frac{4\tau D_L C_S}{\frac{1}{r_1} - \frac{1}{r_2}} \left[1 - e^{-\frac{\pi}{\tau}\left(t - t_{lag}\right)} \right] \tag{19}$$

Where τ is the time constant of the system:

$$\tau = \frac{\frac{D_L}{D_P}\left(1 - \frac{r_2}{r_3} + \ln\frac{r_2}{r_3}\right) + \left(\frac{r_2}{r_1} - 1 - \ln\frac{r_2}{r_1}\right)}{\frac{4\pi D_L}{S}} \tag{20}$$

Where D_L and D_P are the diffusion coefficients of the drug molecules in the liquefied intermediate and polymeric shells, respectively, C_S is the concentration in the drug core assumed constant over time, r_1, r_2 and r_3 are the radiuses of the drug core, intermediate shell and polymeric shell, respectively and S is the surface area of the system ($S = 4\pi r_3^2$). Obtaining the rate of undesired drug release of the drug remaining inside the polymeric shell from the ON state is the main purpose in the modelling of the system in the OFF state. It is supposed that the system is in the OFF state at any arbitrary time t ($t > t_e > t_{lag}$). The fractional release of drug molecules from the polymeric shell as a function of time in the OFF state can be determined as:

$$\frac{M_t'}{M_\infty'} = 1 - e^{\left(\frac{-4\pi D_P}{nS}\right)(t - t_e)} \tag{21}$$

Where M_t' is the cumulative amount of released drug in the OFF state, $M'\infty$ is the the total amount of drug available inside the polymeric shell at the starting time of the OFF state, n is a parameter defined on geometrical characteristic of the system:

$$n = \frac{r_2}{r_3} - \ln\frac{r_2}{r_3} - 1 \tag{22}$$

3. Experimental methods for temperature-dependent model calibration

In the section above, the most common systems exhibiting temperature-dependent drug-release behavior have been described. Across the different modelling strategies proposed in the literature, a recurring feature is the need to determine system-specific parameters experimentally for each case under investigation. Since the aim of this review is to provide a comprehensive toolbox for describing thermo-responsive systems, it must therefore also include guidance on how to experimentally evaluate all the parameters required by these models. A variety of experimental techniques can be employed to explore how

temperature affects nanoparticle size, polymer–solvent interactions, matrix structure, and ultimately drug-release kinetics. These methods are essential not only for identifying key thermal transition points such as LCST, UCST, or lipid melting temperature but also for quantifying the parameters that enter mechanistic models. In practice, the choice of technique depends on the specific system under investigation: polymeric micelles, lipid-based nanocarriers, and degradable particles each require different characterization approaches. The following subsection summarizes the most widely used experimental tools for characterizing thermo-responsiveness. The goal here is to highlight which measurements are most relevant for parameterizing mathematical models and how they inform the physical interpretation of temperature-dependent release. A comprehensive summary is presented in Table 5.

3.1. Nanoparticle size and geometry

A central aspect of thermo-responsive nanocarriers is the way their size and morphology evolve with temperature. Many of the modelling approaches discussed in this review treat particle radius, shell thickness, and internal structure as key parameters that directly influence the effective diffusion distance and the accessibility of different transport pathways. Since these geometrical properties often change with temperature, they must be quantified experimentally under the same thermal conditions used in release modelling. Among the available techniques, Dynamic Light Scattering (DLS) is by far the most widely used tool for monitoring temperature-dependent changes in nanoparticle size [184]. DLS measures the fluctuations in scattered light intensity caused by the Brownian motion of the particles and, through the Stokes–Einstein equation, provides an estimate of their hydrodynamic diameter, which reflects not only the polymeric structure but also the solvation layer [169]. By performing temperature-controlled DLS measurements, it is possible to obtain size–temperature profiles that capture swelling, deswelling, collapse transitions characteristic of thermo-responsive systems [185]. For LCST-type polymers, for example, DLS typically reveals a sharp decrease in hydrodynamic radius at the transition temperature [127], while in degradable matrices a more gradual radius change may be observed [186]. Beyond simple diameter estimation, DLS can also provide information on polydispersity index (PDI) and the presence of aggregates or structural rearrangements that may occur across thermal transitions [187]. A rise in PDI upon heating, for instance, can indicate the onset of partial aggregation or heterogeneous collapse features that are important for interpreting deviations from ideal modelling assumptions such as homogeneous particle structure. From a modelling perspective, the temperature-dependent particle radius R(T) obtained from DLS directly feeds into the geometrical terms of diffusion equations, affecting factors such as diffusion path length, surface-to-volume ratio, and shell thickness in core–shell configurations.

In models based on the Pontrelli et al. [142] framework, for example, changes in R(T) or shell thickness with temperature modify both boundary conditions and internal diffusion domains, thereby influencing dissolution and release kinetics. Consequently, DLS provides essential quantitative input for mechanistic models aiming to incorporate thermo-responsive size transitions in a physically meaningful way. It is important to note that the size obtained from DLS corresponds to the hydrodynamic diameter, which includes not only the polymeric core but also the surrounding solvation layer [170]. In thermo-responsive systems, this quantity is inherently temperature-dependent and reflects changes in polymer hydration, chain conformation, and solvent quality. As a result, DLS measurements may not represent a fixed geometric particle size, but rather an effective, dynamic dimension that varies between swollen (below LCST) and collapsed (above LCST) states [144]. While DLS provides rapid and quantitative information on temperature-dependent size variations, a complete understanding of thermo-responsive nanocarriers also requires direct visualization of their internal morphology. Transmission Electron Microscopy (TEM) and, more specifically, cryogenic TEM (cryo-TEM) are indispensable tools for this purpose, as they allow the nanoscale structure of the particles to be imaged with high spatial resolution [145,188]. These techniques provide information that cannot be captured by scattering-based methods alone, including particle shape, internal compartmentalization, shell thickness, and morphological changes induced by temperature [144,189]. Conventional TEM is typically performed on dried samples and is therefore well suited for revealing core–shell architectures, polymer density gradients, or distinct domains within block-copolymer assemblies. In thermo-responsive systems, TEM imaging can be used to assess whether heating induces structural rearrangements such as shell compaction, partial collapse of the corona, or aggregation into larger superstructures. For degradable nanocarriers, TEM can also capture erosion patterns, pore formation, and fragmentation of the matrix, offering valuable insights into the structural consequences of hydrolytic or enzymatic degradation [190]. Cryo-TEM, by contrast, allows nanoparticles to be imaged in a vitrified, fully hydrated state, preserving their native morphology and avoiding drying artefacts [191,192].

This makes cryo-TEM particularly powerful for characterizing temperature-dependent transitions in aqueous environments, such as the coil–globule collapse of LCST/UCST polymers or the reorganization of lipid bilayers in thermosensitive liposomes. By preparing samples at different temperatures immediately prior to vitrification, it is possible to capture snapshots of the system across its thermal transition, revealing changes in shell thickness, core density, internal ordering, or the presence of phase-separated domains. These structural fingerprints help validate whether the assumed geometrical representations used in modelling such as spherical symmetry, uniform shell thickness, or homogeneous density are consistent with the real system. In combination with DLS, cryo-TEM/TEM provides a robust structural dataset for informing mechanistic models. Whereas DLS yields the hydrodynamic radius R(T), microscopy reveals the true physical radius, the core–shell thicknesses, and the spatial distribution of polymer segments, all of which are critical for defining the diffusion domains used in continuum formulations. For example, the shell thickness measured via cryo-TEM can be directly incorporated into the model as the width of the diffusion–reaction layer, while temperature-induced densification observed in images can justify changes in the effective diffusivity or porosity of the shell. Thus, cryo-TEM/TEM serve as essential complementary techniques for translating the structural dynamics of thermo-responsive carriers into quantitatively grounded model parameters.

3.2. Polymer-solvent thermodynamics

Thermo-responsive drug-delivery systems fundamentally rely on how polymer–solvent interactions evolve with temperature. These interactions determine whether a polymer remains fully hydrated and expanded or instead collapses into a compact, poorly solvated state. Because the Flory–Huggins interaction parameter χ_{FH} and its temperature dependence cannot be measured directly, experimental thermodynamic characterization must rely on observable data that reflect changes in polymer solubility.

The key measurable quantity is the liquid–liquid coexistence (binodal) curve, constructed from cloud-point temperatures. When phase separation begins, the system reaches the cloud-point composition, yet the equilibrium phase on the opposite side of the tie line appears only in infinitesimal amounts meaning its composition cannot be directly sampled, making experimental determination of the full binodal unfeasible. The most common approach consists in enforcing the equality of chemical potentials at each experimentally measured composition. In this framework, the problem reduces to solving a system of two equations with two unknowns, allowing the determination of the corresponding composition of the coexisting phase at the same temperature, together with the value of the Flory–Huggins interaction parameter, χ_{FH}, at that temperature. By repeating this procedure for all available experimental data points, the temperature and composition dependence of χ_{FH} can be reconstructed. An alternative strategy consists in the

computational reconstruction of the binodal curve by interpolating the experimentally accessible cloud-point data. This can be achieved using suitable mathematical representations, such as polynomial fitting, spline interpolation, or parametric fitting routines implemented in numerical environments such as MATLAB. This interpolation effectively recreates the full binodal curve, allowing every experimentally measured composition to be paired with its corresponding equilibrium composition on the opposite branch. Once these reconstructed coexistence points are available, the equilibrium conditions can be applied as explained in section 2.2.2.1. By imposing equality of the polymer's chemical potential across the two phases and solving the resulting system of equations, the adjustable parameters appearing in $\chi_{FH}(T, \phi)$ can be identified. In this way, experimental phase-behavior data become quantitatively linked to the thermodynamic model, enabling χ_{FH} to be evaluated consistently and ultimately allowing its temperature dependence to be incorporated into mechanistic descriptions of thermo-responsive drug release. UV–Vis turbidimetry is the most commonly employed method for determining the cloud point (Tcp) temperature and building the liquid-liquid coexistence curve of thermo-responsive polymer solutions.

Its widespread use is largely due to the simplicity and accessibility of the technique: the measurements can be carried out using a standard UV–Vis spectrophotometer equipped with temperature control. To perform the measurement, a polymer solution is prepared in water, transferred into a suitable cuvette, and placed in the spectrometer. A controlled heating program is then applied, during which the transmittance of light through the solution is continuously monitored. As the temperature surpasses the Tcp, phase separation occurs: polymer-rich droplets form and become dispersed in the polymer dilute continuous phase. These droplets scatter incident light, resulting in a sharp drop in transmittance. A critical aspect of turbidimetry is defining which point on the transmittance curve corresponds to the Tcp. The literature presents various definitions, including the onset of transmittance decline, the temperature at 80% or 50% transmittance, and the inflection point of the turbidity curve [146]. The Tcp can be measured across a range of polymer concentrations, plotting the observed Tcp values against concentration gives the cloud point curve, which reflects how phase behavior varies with composition. By monitoring the transmittance of a polymer solution while the temperature is gradually increased or decreased, one can quantify the temperature at which the system undergoes a coil–globule transition, phase separation, or aggregation which are all manifestations of a rising χ_{FH} that renders polymer–solvent interactions unfavorable. For modelling purposes, cloud-point curves allow the reconstruction of qualitative or semi-quantitative χ_{FH} profiles, helping identify the temperature range in which solubility changes are most significant. Turbidimetry therefore serves as a practical link between thermodynamics and model inputs such as polymer solubility, swelling behavior, and discontinuities in diffusivity. In addition to size measurements, DLS can track the intensity of scattered light as a function of temperature. During the coil-to-globule transition, a sharp rise in scattering intensity is typically observed, due to the fact that the intensity is proportional to the sixth power of particle diameter ($I \propto d^6$), according to the Rayleigh approximation. This increase in particle size is accompanied by a rise in the refractive index contrast between the concentrated (dispersed) phase and the surrounding dilute phase, further enhancing scattering.

In contrast, hydrated polymer chains below the Tcp have a refractive index close to that of water, resulting in minimal scattering. As a result, the intensity of scattered light can increase by several orders of magnitude upon heating through the Tcp, making DLS a highly sensitive method for detecting the coil-to-globule transition [193]. The Tcp is determined as the intersection between two linear regressions of the scattering intensity as a function of temperature: one describing the low-temperature baseline corresponding to the homogeneous solution, and the other describing the steep intensity increase observed at higher temperatures due to the onset of aggregation and phase separation [81]. Alternatively, Tcp is often defined as the temperature at which approximately 50% of the aggregation process has occurred, corresponding to the midpoint of the transition [194]. Fig. 8 shows the different approaches for the experimental determination of the cloud point temperature.

3.3. Diffusion and solubility parameters

A critical requirement in the modelling of thermo-responsive carriers is the evaluation of parameters governing drug diffusion and solubility within the nanoparticle matrix. These quantities are sensitive to temperature and must be measured experimentally under well-controlled thermal conditions in order to be used reliably in both empirical/semi-empirical and mechanistic release models. The most common approach involves drug release assays performed at different temperatures, coupled with quantification of the released drug by UV–Vis spectroscopy [147,195,196] or HPLC [148,197,198]. Release experiments can be conducted using dialysis membranes [199,200] or direct sampling of the release medium [201]. By fitting the resulting release profiles with analytical or numerical solutions, ranging from Higuchi-type models to the continuum formulations discussed in Section 2, one can extract effective values of the diffusion coefficients and dissolution rates, as well as infer the solubility-limited release behavior characteristic of many thermo-responsive systems. UV–Vis spectroscopy is one of the most commonly used analytical tools for quantifying drug concentration during release experiments and for determining the temperature dependence of drug solubility. In a typical release study, samples of the external medium are collected over time while the system is maintained at a controlled temperature, and the absorbance of the released drug is measured at its characteristic wavelength [147]. By converting absorbance to concentration using a calibration curve, UV–Vis provides the time-resolved concentration profiles needed to estimate diffusion-related parameters such as the effective diffusivities and dissolution rates. Because measurements can be performed at different temperatures, UV–Vis quantification allows the construction of release curves that directly reveal how transport kinetics accelerate, decelerate, or transition across thermal stimuli. UV–Vis spectroscopy is also central for evaluating temperature-dependent drug solubility, typically through equilibrium shake-flask methods [149,202].

By incubating a known excess of drug release medium at a fixed temperature and measuring the concentration of dissolved drug after equilibration, one obtains the saturation concentration required by diffusion–dissolution models such as those introduced in Section 2. High-performance liquid chromatography (HPLC) is the gold-standard technique for quantifying drug concentration in thermo-responsive release studies, particularly when the drug lacks a strong UV–Vis absorbance peak, when multiple species are present, or when degradation products or excipients interfere with optical measurements. In a typical temperature-controlled release experiment, aliquots of the release medium are periodically withdrawn and injected into the HPLC system. By separating the analyte from other formulation components, HPLC enables accurate determination of the released drug even in complex matrices or at low concentrations. As with UV–Vis, fitting the resulting concentration–time profiles provides access to the diffusion-related parameters required by drug release models.

3.4. Thermal transition parameters

Differential Scanning Calorimetry (DSC) is the primary technique for identifying thermally induced phase transitions in both polymeric and lipid-based nanocarriers [150]. DSC quantifies the heat flow associated with endothermic or exothermic transitions, enabling precise lipid phase transitions that govern permeability in thermosensitive liposomes [203]. These measurements provide direct insight into the cooperativity and enthalpy of thermal events, which in turn inform the abruptness or gradualness of parameter changes (e.g., radius collapse, diffusivity shifts) that must be introduced into mathematical models. For lipid-

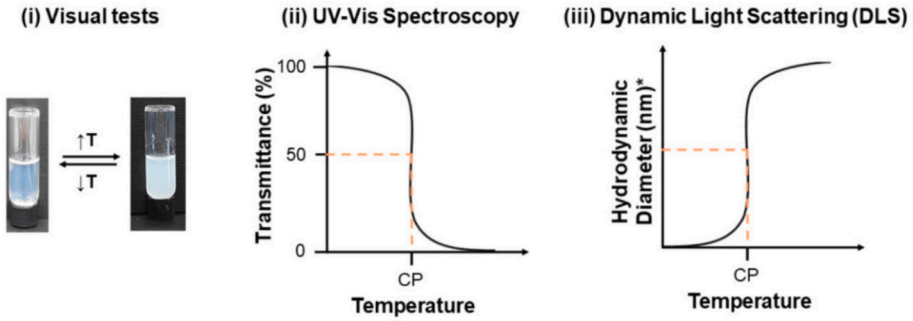

Fig. 8. Determination of the cloud point (Tcp) by (i) visual tests, as the temperature at which the solution turns cloudy, (ii) UV–Vis spectroscopy, as the temperature at which the transmittance drops to 50%, and (iii) dynamic light scattering (DLS), as the temperature at which 50% aggregation occurs. Reprinted with permission from [194].

based carriers DSC measurements reveal the melting temperature (Tm) of the bilayer, a critical parameter for modelling the steep temperature-driven increase in membrane permeability. Repeated DSC heating and cooling cycles can also assess the reversibility of the transition, an important consideration when modelling systems subjected to thermal cycling or intermittent hyperthermia [204].

4. Perspectives and outlooks

4.1. Continuum and multiphysics thermo-release models

Recent work demonstrates that continuum-scale and multiphysics models are becoming increasingly powerful tools for predicting temperature-dependent drug release under realistic physiological conditions [205,206]. For thermosensitive liposomes (TSLs), numerical frameworks now couple heat transfer, membrane phase transitions, drug diffusion, and vascular transport into a unified description of heat-triggered release. Adabbo et al. [206] quantified doxorubicin release from TSLs by integrating temperature-dependent permeability with spatial heat propagation, producing predictive release profiles under hyperthermic conditions. Even more sophisticated approaches have been proposed for focused ultrasound (FUS) enhanced delivery: Moradi Kashkooli et al. [207] developed a spatiotemporal computational model incorporating FUS-induced heating, blood perfusion, nanoparticle kinetics, and tissue drug transport, enabling simulation of drug bioavailability in solid tumors under realistic thermal fields. A 2025 multiphysics extension further integrates thermal dynamics, liposome melting, and systemic circulation, offering a full in silico platform for evaluating the performance of TSL-based treatments under patient-specific conditions [208]. These studies illustrate a clear trajectory: continuum and multiphysics models are evolving from idealized in vitro descriptions toward biologically structured simulations that incorporate spatially heterogeneous heating, vascular clearance, and tissue-level barriers: elements that will be critical for future temperature-dependent drug-release modelling.

4.2. Artificial intelligence (AI)/machine learning (ML)-driven design for stimuli-responsive nanomaterials

Machine-learning and data-driven strategies are becoming increasingly relevant for the design and optimization of stimuli-responsive soft materials, including systems whose behavior is modulated by temperature [209–212]. Ejeromedoghene and coworkers [213] reviewed the rapid emergence of ML methods in the design of 3D/4D-printed hydrogels capable of responding to external stimuli such as temperature, showing how algorithms can identify structure–function relationships, optimize responsiveness, and accelerate materials discovery in ways that conventional trial-and-error approaches cannot match. At a broader biomedical scale, multi-scale modelling reviews highlight the growing role of AI in nanomedicine, where machine-learning models are increasingly used to predict nanoparticle transport, tumor penetration, and spatiotemporal therapeutic response from high-dimensional biological and physicochemical data [214–217]. Debnath and co-workers [218] emphasize that integrating AI with physics-based models can overcome long-standing barriers in nano-cancer therapy, enabling rapid screening of nanoparticle design variables and improved prediction of in vivo performance across multiple scales of biological complexity. A future in which temperature-dependent release models are integrated into hybrid ML–physics frameworks, capable of inferring optimal nanocarrier architectures and predicting thermal responsiveness across diverse physiological conditions, should be regarded as the natural trajectory of the field.

4.3. Molecular dynamics simulations of thermo-responsive behavior

At the molecular scale, recent simulation studies show that all-atom and coarse-grained molecular dynamics (MD) can capture the fundamental temperature-dependent transitions that govern thermo-responsive behavior in soft nanomaterials [211].

Hopkins and Blaisten-Barojas [219] demonstrated that PNIPAM and PDEA undergo clear coil–globule transitions in aqueous and mixed solvents, with MD simulations revealing the molecular hydration changes and structural rearrangements responsible for thermo-responsiveness. Tavagnacco and coworkers [126,220] used MD simulations with different water models to reproduce PNIPAM's temperature-dependent solution behavior, showing how molecular-level restructuring of hydration layers can be linked to macroscopic phase behavior and collapse temperatures relevant for drug-release modulation. Fig. 9 shows the temperature-induced coil-to-globule transition of the PNIPAM chain. As temperature increases, the radius of gyration decreases, indicating chain collapse, while the SASA shifts to lower values, reflecting reduced hydration. The snapshot at 303 K confirms the compact, collapsed conformation. Extending beyond single-chain behavior, recent MD work on crosslinked PNIPAM hydrogels under hydrothermal conditions has characterized how temperature shifts water capture, network swelling, and polymer mobility properties that directly influence diffusion and release in thermo-responsive matrices [221]. These studies demonstrate that molecular simulation is now mature enough to resolve the nanoscale physics hydration, collapse, density changes, membrane interactions that underlie temperature-dependent transitions. Soon, such simulations could directly supply temperature-dependent parameters (e.g., $\chi_{FH}(T)$, polymer density, permeability, solute diffusivity) to continuum drug-release models, enabling genuinely multiscale thermo-responsive design frameworks.

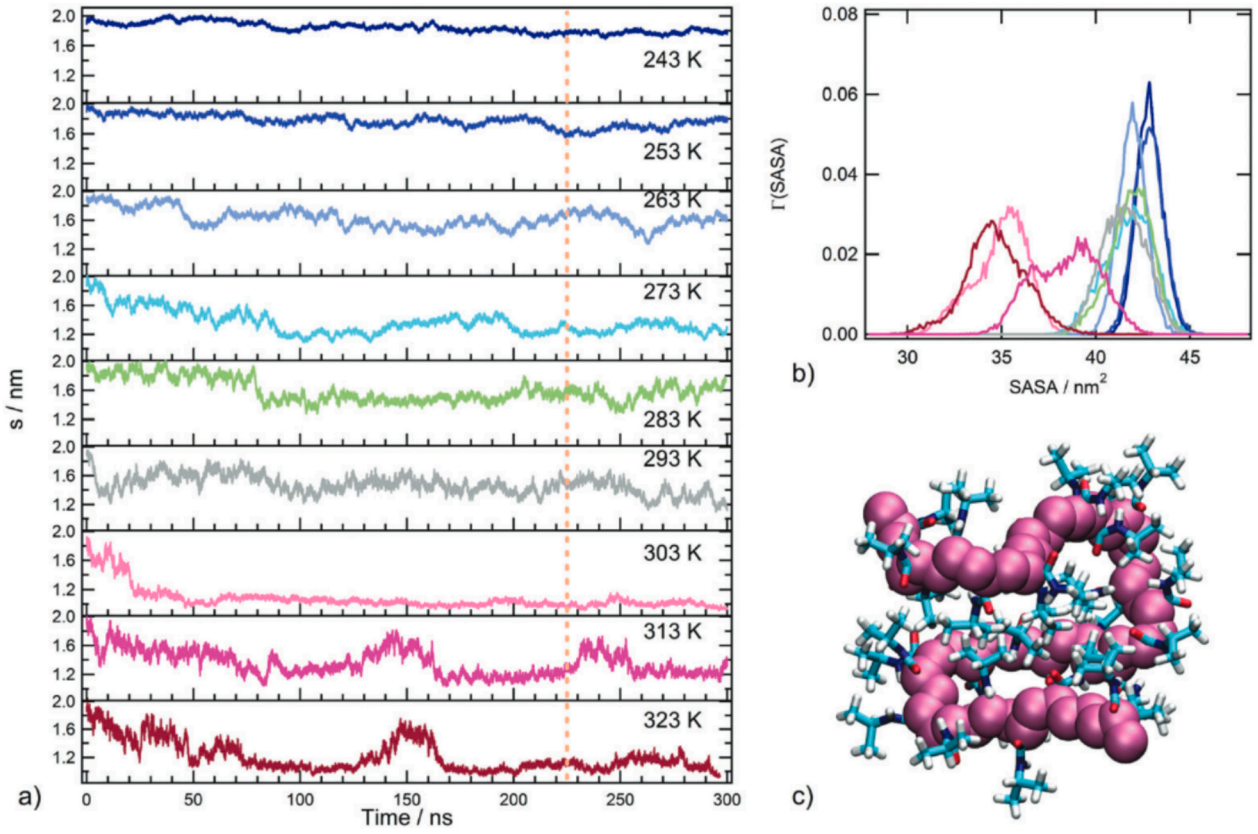

Fig. 9. (a) Time evolution of the radius of gyration of the PNIPAM chain at different temperatures (243–323 K); dashed lines indicate the analysis window. (b) Distributions of solvent-accessible surface area (SASA) as a function of temperature. (c) MD snapshot at 303 K showing the collapsed conformation of the PNIPAM chain. Reprinted with permission from [126].

5. Conclusions

Thermo-responsive polymeric nanoparticles have evolved from proof-of-concept smart materials into highly tunable platforms capable of delivering drugs with a unique level of temporal and spatial control. As highlighted throughout this review, temperature should no longer be regarded as a passive external variable that merely accelerates diffusion or degradation processes. Instead, it acts as a true design parameter that governs nanocarrier behavior through well-defined physicochemical mechanisms. Across different classes of thermo-responsive systems, drug release can be consistently interpreted in terms of three fundamental and often concurrent mechanisms: the temperature-dependent kinetics of matrix degradation or erosion, the modulation of mass transport through temperature-sensitive diffusion and solubility, and the activation of switch-like release events driven by thermo-induced structural transitions.

Recognizing and disentangling these mechanisms is essential for moving beyond empirical optimization toward rational design. A central message emerging from this work is that predictive control over thermo-responsive drug release cannot be achieved without explicitly linking temperature to nanocarrier structure and thermodynamics. Models that treat nanoparticle geometry, polymer-solvent interactions, and transport coefficients as fixed quantities are inherently limited when applied to systems that undergo temperature-induced collapse, swelling, phase separation, or membrane melting. In contrast, mechanistic frameworks that integrate polymer thermodynamics, geometry evolution, and coupled transport phenomena provide a physically meaningful route to describing both gradual and sharp modulation of drug release behavior. Such models not only improve interpretability but also enable extrapolation beyond the specific experimental conditions used for calibration. Based on the analysis presented, we advocate a forward-looking design strategy for thermo-responsive nanocarriers in which material synthesis, experimental characterization, and modelling are developed in parallel rather than sequentially. In this approach, polymer chemistry is selected to define the desired thermal transition, experimental techniques are used to quantitatively map temperature-dependent size, solubility, and transport properties, and mechanistic models are employed to translate these inputs into predictive release profiles. This integrated method allows thermo-responsiveness to be engineered deliberately rather than observed a posteriori, paving the way for nanocarriers whose behavior can be tuned with precision across physiological and externally applied temperature ranges. Looking ahead, the convergence of thermo-responsive materials with continuum multiphysics modelling, molecular simulations, and data-driven design tools is expected to further accelerate progress in the field. By embedding temperature-dependent release mechanisms within multiscale and predictive frameworks, thermo-responsive nanoparticles can be transformed into truly programmable delivery systems. In this context, the rational modulation of drug release through temperature is not simply a functional advantage, but a foundational principle for the next generation of smart nanomedicine.

CRediT authorship contribution statement

Marcello Schifone: Writing – original draft, Investigation. **Giuseppe Nunziata:** Writing – original draft, Investigation. **Filippo Rossi:** Writing – review & editing, Supervision.

Declaration of competing interest

The authors declare that they have no known competing financial interests or personal relationships that could have appeared to influence the work reported in this paper.

Data availability

Data will be made available on request.

References

[1] Hu S, Zhao R, Shen Y, Lyu B. Revolutionizing drug delivery: the power of stimulus-responsive nanoscale systems. Chem Eng J 2024;496:154265. https://doi.org/10.1016/j.cej.2024.154265.

[2] Beach MA, Nayanathara U, Gao Y, Zhang C, Xiong Y, Wang Y, et al. Polymeric nanoparticles for drug delivery. Chem Rev 2024;124:5505–616. https://doi.org/10.1021/acs.chemrev.3c00705.

[3] Jadhav V, Roy A, Kaur K, Rai AK, Rustagi S. Recent advances in nanomaterial-based drug delivery systems. Nano-Struct Nano-Objects 2024;37:101103. https://doi.org/10.1016/j.nanoso.2024.101103.

[4] Liu X, Zhou Q, Yang Y, Wu X, Chen J, Wang R, et al. Hydrogels in cancer treatment: mapping the future of precision drug delivery. Front Immunol 2025;16. https://doi.org/10.3389/fimmu.2025.1607240.

[5] Liu B, Chen K, Liu B, Chen K. Advances in hydrogel-based drug delivery systems. Gels 2024;10. https://doi.org/10.3390/gels10040262.

[6] Li X, Li L, Wang D, Zhang J, Yi K, Su Y, et al. Fabrication of polymeric microspheres for biomedical applications. Mater Horiz 2024;11:2820–55. https://doi.org/10.1039/D3MH01641B.

[7] Yang S, Wu H, Peng C, He J, Pu Z, Lin Z, et al. From the microspheres to scaffolds: advances in polymer microsphere scaffolds for bone regeneration applications. Biomater Transl 2024;5:274–99. https://doi.org/10.12336/biomatertransl.2024.03.005.

[8] Afzal O, Altamimi ASA, Nadeem MS, Alzarea SI, Almalki WH, Tariq A, et al. Nanoparticles in drug delivery: from history to therapeutic applications. Nanomaterials 2022;12:4494. https://doi.org/10.3390/nano12244494.

[9] Alavi SE, Alharthi S, Alavi SZ, Raza A, Ebrahimi Shahmabadi H. Bioresponsive drug delivery systems. Drug Discov Today 2024;29:103849. https://doi.org/10.1016/j.drudis.2023.103849.

[10] Fang Z, Zhang H, Guo J, Guo J. Overview of therapeutic drug monitoring and clinical practice. Talanta 2024;266:124996. https://doi.org/10.1016/j.talanta.2023.124996.

[11] Kurul F, Turkmen H, Cetin AE, Topkaya SN. Nanomedicine: how nanomaterials are transforming drug delivery, bio-imaging, and diagnosis. Next Nanotechnol 2025;7:100129. https://doi.org/10.1016/j.nxnano.2024.100129.

[12] Tripathi D, Pandey P, Sharma S, Rai AK, Prabhu BHM. Advances in nanomaterials for precision drug delivery: insights into pharmacokinetics and toxicity. Bioimpacts 2024;15:30573. https://doi.org/10.34172/bi.30573.

[13] Teixeira do Nascimento A, Stoddart PR, Goris T, Kael M, Manasseh R, Alt K, et al. Stimuli-responsive materials for biomedical applications. Adv Mater 2025;37:e07559. https://doi.org/10.1002/adma.202507559.

[14] Dai X, Li W-J, Xie D-D, Liu B, Gong L, Han H-H. Stimuli-responsive nano drug delivery systems for the treatment of neurological diseases. Small 2025;21:2410030. https://doi.org/10.1002/smll.202410030.

[15] Zheng R, Yu C, Yao D, Cai M, Zhang L, Ye F, et al. Engineering stimuli-responsive materials for precision medicine. Small 2025;21:2406439. https://doi.org/10.1002/smll.202406439.

[16] Asif Iqbal M, Mahmood A, Al-Masry W, Ho Park C, Ul Hassan S, Akhter T. Versatile poly(n-vinylcaprolactam)- grafted -hydroxypropyl cellulose polymers with tailored thermo- and pH-responsive properties via sustainable organocatalyzed atom transfer radical polymerization. Polym Chem 2024;15:4244–54. https://doi.org/10.1039/D4PY00931B.

[17] Lacroce E, Nunziata G, Cianniello F, Limiti E, Rainer A, Vangosa FB, et al. Amphiphilic pH-responsive core-shell nanoparticles can increase the performances of cellulose-based drug delivery systems. Int J Biol Macromol 2024;283:137659. https://doi.org/10.1016/j.ijbiomac.2024.137659.

[18] Lacroce E, Pizzetti F, Urrego NMB, Nunziata G, Masi M, Rossi F. Magnetically active bicontinuous polymer structures for multiple controlled drug delivery. Macromol Biosci 2024;24:2400084.

[19] Nunziata G, Nava M, Lacroce E, Pizzetti F, Rossi F. Thermo-responsive polymer-based nanoparticles: from chemical design to advanced applications. Macromol Rapid Commun 2025;46:2401127. https://doi.org/10.1002/marc.202401127.

[20] Darvishi A, Ansari M. Thermoresponsive and supramolecular polymers: interesting biomaterials for drug delivery. Biotechnol J 2024;19:e202400379. https://doi.org/10.1002/biot.202400379.

[21] Trucillo P. Biomaterials for drug delivery and human applications. Materials 2024;17. https://doi.org/10.3390/ma17020456.

[22] Geszke-Moritz M, Moritz M, Geszke-Moritz M, Moritz M. Biodegradable polymeric nanoparticle-based drug delivery systems: comprehensive overview, perspectives and challenges. Polymers 2024;16. https://doi.org/10.3390/polym16172536.

[23] Wang R, Liao W, Wang X, Chen L, Zhao X, Xing J, et al. Thermoresponsive nanofiber dressing for body heat-triggered drug release and exudate management in chronic wounds. Next Mater 2026;10:101508.

[24] Yu Q, Zhang H, Chen L, Wei X, Xie E, Zhu X, et al. A bioorthogonal click reaction-based platelet-rich plasma delivery system for accelerating wound healing. Acta Biomater 2026;209:322–38.

[25] Xia Y, Ma Z, Wu X, Wei H, Zhang H, Li G, et al. Advances in stimuli-responsive chitosan hydrogels for drug delivery systems. Macromol Biosci 2024;24:2300399. https://doi.org/10.1002/mabi.202300399.

[26] Biswas R, Mondal S, Ansari MA, Sarkar T, Condiuc IP, Trifas G, et al. Chitosan and its derivatives as nanocarriers for drug delivery. Molecules 2025;30. https://doi.org/10.3390/molecules30061297.

[27] Singh S, Rastogi H, Deva V, Dixit R, Gupta T, Tyagi M. Alginate based nanoparticles and its application in drug delivery systems. J Pharm Negat Results 2022:1463–9. https://doi.org/10.47750/pnr.2022.13.S06.195.

[28] Wawszczak A, Kocki J, Kołodyńska D. Alginate as a sustainable and biodegradable material for medical and environmental applications—the case studies. J Biomed Mater Res B Appl Biomater 2024;112:e35475. https://doi.org/10.1002/jbm.b.35475.

[29] Chudzińska J, Wawrzyńczak A, Feliczak-Guzik A, Chudzińska J, Wawrzyńczak A, Feliczak-Guzik A. Microneedles based on a biodegradable polymer—hyaluronic acid. Polymers 2024;16. https://doi.org/10.3390/polym16101396.

[30] Raza MA, Sharma MK, Nagori K, Jain P, Ghosh V, Gupta U, et al. Recent trends on polycaprolactone as sustainable polymer-based drug delivery system in the treatment of cancer: biomedical applications and nanomedicine. Int J Pharm 2024;666:124734. https://doi.org/10.1016/j.ijpharm.2024.124734.

[31] Mundel R, Thakur T, Chatterjee M. Emerging uses of PLA–PEG copolymer in cancer drug delivery. 3 Biotech 2022;12:41. https://doi.org/10.1007/s13205-021-03105-y.

[32] Shekhar N, Mondal A. Synthesis, properties, environmental degradation, processing, and applications of polylactic acid (PLA): an overview. Polym Bull 2024;81:11421–57. https://doi.org/10.1007/s00289-024-05252-7.

[33] Yang J, Zeng H, Luo Y, Chen Y, Wang M, Wu C, et al. Recent applications of PLGA in drug delivery systems. Polymers (Basel) 2024;16:2606. https://doi.org/10.3390/polym16182606.

[34] Throat S, Bhattacharya S. Macromolecular poly(N-isopropylacrylamide) (PNIPAM) in cancer treatment and beyond. Adv Polym Technol 2024;2024:1444990. https://doi.org/10.1155/2024/1444990.

[35] Mohan A, Santhamoorthy M, Phan TTV, Kim S-C, Mohan A, Santhamoorthy M, et al. PNIPAm-based pH and thermoresponsive copolymer hydrogel for hydrophobic and hydrophilic drug delivery. Gels 2024;10. https://doi.org/10.3390/gels10030184.

[36] Pathan I, Raza MA, Roy A, Badwaik H, Sakure K, uddin A. Recent advances in thermo-responsive hydrogels for ocular drug delivery: materials, mechanisms, and clinical potential. J Drug Delivery Sci Technol 2025;114:107537. https://doi.org/10.1016/j.jddst.2025.107537.

[37] Jo S, Roh S, Shim J, Yu JW, Jung Y, Jang WY, et al. Modulating the thermoresponsive characteristics of PLGA–PEG-PLGA hydrogels via manipulation of PLGA monomer sequences. Biomacromolecules 2024;25:5374–86. https://doi.org/10.1021/acs.biomac.4c00817.

[38] Singh A, Dowdall N, Hoare T. Poly(oligo(ethylene glycol) methacrylate)-based polymers in biomedical applications: preparation and applications. Biomacromolecules 2025;26:3929–73. https://doi.org/10.1021/acs.biomac.5c00145.

[39] Begines B, Ortiz T, Pérez-Aranda M, Martínez G, Merinero M, Argüelles-Arias F, et al. Polymeric nanoparticles for drug delivery: recent developments and future prospects. Nanomaterials 2020;10. https://doi.org/10.3390/nano10071403.

[40] Nunziata G, Limiti E, Aramini D, Nava M, Moretti L, Rainer A, et al. PH-Thermo dual-responsive polymeric nanoparticles for womens health: dual action against cervical and ovarian cancer cells. ACS Appl Mater Interfaces 2025;17:61888–904.

[41] Shi Y, Zhang Y, Zhu L, Miao Y, Zhu Y, Yue B. Tailored drug delivery platforms: stimulus-responsive core–shell structured nanocarriers. Adv Healthc Mater 2024;13:2301726. https://doi.org/10.1002/adhm.202301726.

[42] Budharaju H, Chandrababu H, Zennifer A, Chellappan D, Sethuraman S, Sundaramurthi D. Tuning thermoresponsive properties of carboxymethyl cellulose (CMC)- agarose composite bioinks to fabricate complex 3D constructs for regenerative medicine. Int J Biol Macromol 2024;260:129443.

[43] Gao G, Shu P, Tan Y, Zheng T, Fan W, Lu L, et al. Preclinical development and phase i study of ZSYY001, a polymeric micellar paclitaxel for advanced solid tumor. Cancer Med 2025;14:e71039. https://doi.org/10.1002/cam4.71039.

[44] Fang R, Liu M, Jiang L. Design of nanoparticle systems by controllable assembly and temporal/spatial regulation. Adv Funct Mater 2020;30:1903351. https://doi.org/10.1002/adfm.201903351.

[45] Zheng S, Zou X, Wei Y, Cui X, Cai S, Li X, et al. Phytochemical-loaded thermo-responsive liposome for synergistic treatment of methicillin-resistant *Staphylococcus aureus* infection. Biomater Res 2025;29:0159.

[46] Nunziata G, Pizzetti F, Veglianese P, Forloni G, Balducci C, Rossi F. Can nanoparticle-based intranasal delivery systems revolutionize treatment of central nervous system diseases? Expert Opin Drug Deliv 2026;23:7–11.

[47] Abuwatfa WH, Awad NS, Pitt WG, Husseini GA, Abuwatfa WH, Awad NS, et al. Thermosensitive polymers and thermo-responsive liposomal drug delivery systems. Polymers 2022;14. https://doi.org/10.3390/polym14050925.

[48] Dobó DG, Németh Z, Sipos B, Cseh M, Pallagi E, Berkesi D, et al. Pharmaceutical development and design of thermosensitive liposomes based on the QbD approach. Molecules 2022;27. https://doi.org/10.3390/molecules27051536.

[49] Nunziata G, Pollonio D, Lacroce E, Rossi F. Smart pH-responsive polymers in biomedical applications: nanoparticles, hydrogels, and emerging hybrid platforms. Mater Today Chem 2025;49:103063.

[50] Alshawwa SZ, Kassem AA, Farid RM, Mostafa SK, Labib GS, Alshawwa SZ, et al. Nanocarrier drug delivery systems: characterization, limitations, future perspectives and implementation of artificial intelligence. Pharmaceutics 2022;14. https://doi.org/10.3390/pharmaceutics14040883.

[51] Gómez-Lázaro L, Martín-Sabroso C, Aparicio-Blanco J, Torres-Suárez AI, Gómez-Lázaro L, Martín-Sabroso C, et al. Assessment of in vitro release testing methods

for colloidal drug carriers: the lack of standardized protocols. Pharmaceutics 2024;16. https://doi.org/10.3390/pharmaceutics16010103.
[52] Siepmann J, Siepmann F. Mathematical modeling of drug delivery. Int J Pharm 2008;364:328–43. https://doi.org/10.1016/j.ijpharm.2008.09.004.
[53] Siepmann J, Siegel RA, Siepmann F. Diffusion controlled drug delivery systems. In: Siepmann J, Siegel RA, Rathbone MJ, editors. Fundamentals and applications of controlled release drug delivery. Boston, MA: Springer US; 2012. p. 127–52. https://doi.org/10.1007/978-1-4614-0881-9_6.
[54] Lawai V, Ngaini Z, Farooq S, Wahi R, Bhawani SA. Current advances in molecularly imprinted polymers and their release mechanisms in drug delivery systems. Polym Adv Technol 2024;35:e6317. https://doi.org/10.1002/pat.6317.
[55] Bărăian A-I, Iacob B-C, Bodoki AE, Bodoki E, Bărăian A-I, Iacob B-C, et al. In vivo applications of molecularly imprinted polymers for drug delivery: a pharmaceutical perspective. Int J Mol Sci 2022;23. https://doi.org/10.3390/ijms232214071.
[56] Lao LL, Peppas NA, Boey FYC, Venkatraman SS. Modeling of drug release from bulk-degrading polymers. Int J Pharm 2011;418:28–41. https://doi.org/10.1016/j.ijpharm.2010.12.020.
[57] Siepmann J, Faisant N, Akiki J, Richard J, Benoit JP. Effect of the size of biodegradable microparticles on drug release: experiment and theory. J Control Release 2004;96:123–34. https://doi.org/10.1016/j.jconrel.2004.01.011.
[58] Guo F, Du Y, Wang Y, Wang M, Wang L, Yu N, et al. Targeted drug delivery systems for matrix metalloproteinase-responsive anoparticles in tumor cells: A review. Int J Biol Macromol 2024;257:128658. https://doi.org/10.1016/j.ijbiomac.2023.128658.
[59] Nelemans LC, Gurevich L. Drug delivery with polymeric nanocarriers—cellular uptake mechanisms. Materials 2020;13:366. https://doi.org/10.3390/ma13020366.
[60] Lv Y, Li W, Liao W, Jiang H, Liu Y, Cao J, et al. Nano-drug delivery systems based on natural products. Int J Nanomedicine 2024;19:541–69. https://doi.org/10.2147/IJN.S443692.
[61] Casalini T. Not only *in silico* drug discovery: molecular modeling towards *in silico* drug delivery formulations. J Control Release 2021;332:390–417. https://doi.org/10.1016/j.jconrel.2021.03.005.
[62] Jayasinghe MK, Lee CY, Tran TTT, Tan R, Chew SM, Yeo BZJ, et al. The role of in silico research in developing nanoparticle-based therapeutics. Front Digital Health 2022;4. https://doi.org/10.3389/fdgth.2022.838590.
[63] Harkos C, Hadjigeorgiou AG, Voutouri C, Kumar AS, Stylianopoulos T, Jain RK. Using mathematical modelling and AI to improve delivery and efficacy of therapies in cancer. Nat Rev Cancer 2025;25:324–40. https://doi.org/10.1038/s41568-025-00796-w.
[64] Peppas NA, Narasimhan B. Mathematical models in drug delivery: how modeling has shaped the way we design new drug delivery systems. J Control Release 2014;190:75–81. https://doi.org/10.1016/j.jconrel.2014.06.041.
[65] Mathematical models of drug release, strategies to modify the drug release from pharmaceutical systems. ResearchGate n.d. https://www.researchgate.net/publication/311344504_Mathematical_models_of_drug_release_strategies_to_modify_the_drug_release_from_pharmaceutical_systems (accessed November 7, 2025).
[66] Ritger PL, Peppas NA. A simple equation for description of solute release I. Fickian and non-fickian release from non-swellable devices in the form of slabs, spheres, cylinders or discs. J Control Release 1987;5:23–36. https://doi.org/10.1016/0168-3659(87)90034-4.
[67] Korsmeyer RW, Gurny R, Doelker E, Buri P, Peppas NA. Mechanisms of solute release from porous hydrophilic polymers. Int J Pharm 1983;15:25–35. https://doi.org/10.1016/0378-5173(83)90064-9.
[68] Xu Y, Jia Y, Wang Z, Wang Z. Mathematical modeling and finite element simulation of slow release of drugs using hydrogels as carriers with various drug concentration distributions. J Pharm Sci 2013;102:1532–43. https://doi.org/10.1002/jps.23497.
[69] Grassi M, Lamberti G, Cascone S, Grassi G. Mathematical modeling of simultaneous drug release and *in vivo* absorption. Int J Pharm 2011;418:130–41. https://doi.org/10.1016/j.ijpharm.2010.12.044.
[70] Wang Y, Zhang K, Qin X, Li T, Qiu J, Yin T, et al. Biomimetic nanotherapies: red blood cell based core-shell structured nanocomplexes for atherosclerosis management. Adv Sci (Weinh) 2019;6:1900172. https://doi.org/10.1002/advs.201900172.
[71] Barratt G, Puisieux F. Takeru higuchi, the man and the scientist. Int J Pharm 2011;418:3–5. https://doi.org/10.1016/j.ijpharm.2011.05.019.
[72] Higuchi T. Physical chemical analysis of percutaneous absorption process from creams and ointments. J Soc Cosmet Chem 1960;11:85–97.
[73] Higuchi T. Rate of release of medicaments from ointment bases containing drugs in suspension. J Pharm Sci 1961;50:874–5. https://doi.org/10.1002/jps.2600501018.
[74] Higuchi T. Mechanism of sustained-action medication. Theoretical analysis of rate of release of solid drugs dispersed in solid matrices. J Pharm Sci 1963;52:1145–9. https://doi.org/10.1002/jps.2600521210.
[75] Porbaha P, Ansari R, Kiafar MR, Bashiry R, Khazaei MM, Dadbakhsh A, et al. A comparative mathematical analysis of drug release from lipid-based nanoparticles. AAPS PharmSciTech 2024;25:208. https://doi.org/10.1208/s12249-024-02922-7.
[76] Trucillo P. Drug carriers: A review on the most used mathematical models for drug release. Processes 2022;10:1094. https://doi.org/10.3390/pr10061094.
[77] Malekjani N, Jafari SM. Modeling the release of food bioactive ingredients from carriers/nanocarriers by the empirical, semiempirical, and mechanistic models. Compr Rev Food Sci Food Saf 2021;20:3–47. https://doi.org/10.1111/1541-4337.12660.
[78] Sawaftah NA, Paul V, Awad N, Husseini GA. Modeling of anti-Cancer drug release kinetics from liposomes and micelles: A review. IEEE Trans Nanobiosci 2021;20:565–76. https://doi.org/10.1109/TNB.2021.3097909.
[79] Askarizadeh M, Esfandiari N, Honarvar B, Sajadian SA, Azdarpour A. Kinetic modeling to explain the release of medicine from drug delivery systems. ChemBioEng Rev 2023;10:1006–49. https://doi.org/10.1002/cben.202300027.
[80] Su Y, Zhang B, Sun R, Liu W, Zhu Q, Zhang X, et al. PLGA-based biodegradable microspheres in drug delivery: recent advances in research and application. Drug Deliv 2021;28:1397–418. https://doi.org/10.1080/10717544.2021.1938756.
[81] Ochi Y, Kawakubo R, Van-Pham D-T, Kitamura Y, Nakanishi H, Norisuye T, et al. Phase separation of polymer mixtures induced by light and heat: A comparative study by light scattering. Adv Nat Sci Nanosci Nanotechnol 2015;6:045002. https://doi.org/10.1088/2043-6262/6/4/045002.
[82] Jung JG, Bae YC. Liquid–liquid equilibria of polymer solutions: Flory-huggins with specific interaction. J Polym Sci B Polym Phys 2010;48:162–7. https://doi.org/10.1002/polb.21883.
[83] Osváth Z, Iván B. The dependence of the cloud point, clearing point, and hysteresis of poly(N-isopropylacrylamide) on experimental conditions: the need for standardization of thermoresponsive transition determinations. Macromol Chem Phys 2017;218:1600470. https://doi.org/10.1002/macp.201600470.
[84] Liu J, Guo H, Gao Q, Li H, An Z, Zhang W. Coil–globule transition of a water-soluble polymer. Macromolecules 2022;55:8524–32. https://doi.org/10.1021/acs.macromol.2c01039.
[85] Sala RL, Venâncio T, Camargo ER. Probing the structural dynamics of the coil–globule transition of thermosensitive nanocomposite hydrogels. Langmuir 2021;37:1531–41. https://doi.org/10.1021/acs.langmuir.0c03079.
[86] Lipid-Based Nanoformulations for Drug Delivery: An Ongoing Perspective n.d. https://www.mdpi.com/1999-4923/16/11/1376 (accessed November 25, 2025).
[87] Schönfeldová T, Piller P, Kovacik F, Pabst G, Okur HI, Roke S. Lipid melting transitions involve structural redistribution of interfacial water. J Phys Chem B 2021;125:12457–65. https://doi.org/10.1021/acs.jpcb.1c06868.
[88] Idrees H, Zaidi SZJ, Sabir A, Khan RU, Zhang X, Hassan S. A review of biodegradable natural polymer-based nanoparticles for drug delivery applications. Nanomaterials (Basel) 2020;10:1970. https://doi.org/10.3390/nano10101970.
[89] Elmowafy M, Shalaby K, Elkomy MH, Alsaidan OA, HAM Gomaa, Abdelgawad MA, et al. Polymeric nanoparticles for delivery of natural bioactive agents: recent advances and challenges. Polymers (Basel) 2023;15:1123. https://doi.org/10.3390/polym15051123.
[90] Kučuk N, Primožič M, Knez Ž, Leitgeb M. Sustainable biodegradable biopolymer-based nanoparticles for healthcare applications. Int J Mol Sci 2023;24:3188. https://doi.org/10.3390/ijms24043188.
[91] Dallaev R, Papež N, Allaham MM, Holcman V, Dallaev R, Papež N, et al. Biodegradable polymers: properties, applications, and environmental impact. Polymers 2025;17. https://doi.org/10.3390/polym17141981.
[92] Beilharz S, Debnath MK, Vinella D, Shoffstall AJ, Karayilan M. Advances in injectable polymeric biomaterials and their contemporary medical practices. ACS Appl Bio Mater 2024;7:8076–101. https://doi.org/10.1021/acsabm.4c01001.
[93] Kuperkar K, Atanase LI, Bahadur A, Crivei IC, Bahadur P. Degradable polymeric bio(nano)materials and their biomedical applications: A comprehensive overview and recent updates. Polymers (Basel) 2024;16:206. https://doi.org/10.3390/polym16020206.
[94] Sreena R, Nathanael AJ. Biodegradable biopolymeric nanoparticles for biomedical applications-challenges and future outlook. Materials (Basel) 2023;16:2364. https://doi.org/10.3390/ma16062364.
[95] Tsung T-H, Tsai Y-C, Lee H-P, Chen Y-H, Lu D-W. Biodegradable polymer-based drug-delivery systems for ocular diseases. Int J Mol Sci 2023;24:12976. https://doi.org/10.3390/ijms241612976.
[96] Parente JF, Sousa VI, Marques JF, Forte MA, Tavares CJ. Biodegradable polymers for microencapsulation systems. Adv Polym Technol 2022;2022:4640379. https://doi.org/10.1155/2022/4640379.
[97] Johnson NW, Jiang SY, Patterson SBH, Hinchcliffe T, Vilela F, Yiu HHP. Nanomaterial scaffolds for enzymatic polymer degradation: A tool to advance current biodegradation assessments of polymers in liquid formulation. Biosci Nanotechnol 2025;1:4. https://doi.org/10.1186/s44331-025-00004-4.
[98] Li W, Tang J, Lee D, Tice TR, Schwendeman SP, Prausnitz MR. Clinical translation of long-acting drug delivery formulations. Nat Rev Mater 2022;7:406–20. https://doi.org/10.1038/s41578-021-00405-w.
[99] Samir A, Ashour FH, Hakim AAA, Bassyouni M. Recent advances in biodegradable polymers for sustainable applications. Npj Mater Degrad 2022;6:68. https://doi.org/10.1038/s41529-022-00277-7.
[100] Feltrin F da S, Agner T, Sayer C, Lona LMF. Curcumin encapsulation in functional PLGA nanoparticles: a promising strategy for cancer therapies. Adv Colloid Interf Sci 2022;300:102582. https://doi.org/10.1016/j.cis.2021.102582.
[101] Kesharwani P, Kumar V, Goh KW, Gupta G, Alsayari A, Wahab S, et al. PEGylated PLGA nanoparticles: unlocking advanced strategies for cancer therapy. Mol Cancer 2025;24:205. https://doi.org/10.1186/s12943-025-02410-x.
[102] Gao Y, Joshi M, Zhao Z, Mitragotri S. PEGylated therapeutics in the clinic. Bioeng Transl Med 2024;9:e10600. https://doi.org/10.1002/btm2.10600.
[103] Rabanel J-M, Piec P-A, Landri S, Patten SA, Ramassamy C. Transport of PEGylated-PLA nanoparticles across a blood brain barrier model, entry into neuronal cells and *in vivo* brain bioavailability. J Control Release 2020;328:679–95. https://doi.org/10.1016/j.jconrel.2020.09.042.
[104] Guo C, Yuan H, Wang Y, Feng Y, Zhang Y, Yin T, et al. The interplay between PEGylated nanoparticles and blood immune system. Adv Drug Deliv Rev 2023;200:115044. https://doi.org/10.1016/j.addr.2023.115044.

[105] Lopez-Mitjavila JJ, Palma-Florez S, Lagunas A, Mir M, Samitier J, Rodriguez-Abreu C, et al. PEGylated PLGA nanoparticles prepared from nano-emulsion templates as versatile platforms to cross blood-brain barrier models. J Drug Delivery Sci Technol 2025;110:107057. https://doi.org/10.1016/j.jddst.2025.107057.
[106] Mayer JB, Patil SM, Shin S-H, Yoo J, Won Y-Y. Internal water-induced acceleration, chemical pathways, and contributing factors in the degradation of poly(lactic-co-glycolic acid) (PLGA) microparticles and devices. ACS Biomater Sci Eng 2025;11:3932–48. https://doi.org/10.1021/acsbiomaterials.5c00419.
[107] Wheeler BP, Medd K, Woodworth KE, Davenport Huyer L. Molecular and macroscopic considerations for degradable aliphatic polyester biomaterial design. Biomacromolecules 2025;26:4784–811. https://doi.org/10.1021/acs.biomac.5c00765.
[108] Cavelier S, Dargaville BL, Hutmacher DW. Water interactions in hydrated aliphatic polyester composite scaffolds. Adv Mater n.d.;:e11614. doi:https://doi.org/10.1002/adma.202511614.
[109] Samanta D, Koithan JA, Muliana AH, Pharr M. Effect of mechanical loading on PLGA biodegradation. Polym Degrad Stab 2025;240:111485. https://doi.org/10.1016/j.polymdegradstab.2025.111485.
[110] Zhao D, Zhu T, Li J, Cui L, Zhang Z, Zhuang X, et al. Poly(lactic-*co*-glycolic acid)-based composite bone-substitute materials. Bioact Mater 2021;6:346–60. https://doi.org/10.1016/j.bioactmat.2020.08.016.
[111] Fredenberg S, Wahlgren M, Reslow M, Axelsson A. The mechanisms of drug release in poly(lactic-co-glycolic acid)-based drug delivery systems—A review. Int J Pharm 2011;415:34–52. https://doi.org/10.1016/j.ijpharm.2011.05.049.
[112] Lucero-Acuña A, Gutiérrez-Valenzuela CA, Esquivel R, Guzmán-Zamudio R. Mathematical modeling and parametrical analysis of the temperature dependency of control drug release from biodegradable nanoparticles. RSC Adv 2019;9:8728–39. https://doi.org/10.1039/C9RA00821G.
[113] Xu Y, Kim C-S, Saylor DM, Koo D. Polymer degradation and drug delivery in PLGA-based drug–polymer applications: A review of experiments and theories. J Biomed Mater Res B Appl Biomater 2017;105:1692–716. https://doi.org/10.1002/jbm.b.33648.
[114] Sunazuka Y, Ueda K, Higashi K, Wada K, Moribe K. Mechanistic analysis of temperature-dependent curcumin release from poly(lactic-co-glycolic acid)/poly(lactic acid) polymer nanoparticles. Mol Pharm 2024;21:1424–35. https://doi.org/10.1021/acs.molpharmaceut.3c01066.
[115] Shafiee K, Bazraei S, Mashak A, Mobedi H. The impact of temperature on the formation, release mechanism, and degradation of PLGA-based in-situ forming implants. J Polym Environ 2024;32:3591–608. https://doi.org/10.1007/s10924-023-03173-6.
[116] Sponchioni M, Capasso Palmiero U, Moscatelli D. Thermo-responsive polymers: applications of smart materials in drug delivery and tissue engineering. Mater Sci Eng C 2019;102:589–605. https://doi.org/10.1016/j.msec.2019.04.069.
[117] Clark EA, Lipson JEG. LCST and UCST behavior in polymer solutions and blends. Polymer 2012;53:536–45. https://doi.org/10.1016/j.polymer.2011.11.045.
[118] Shu X. A review of thermoresponsive drug delivery systems based on LCST/UCST polymer nanofibers. J Phys Conf Ser 2023;2539:012032. https://doi.org/10.1088/1742-6596/2539/1/012032.
[119] Le M, Huang W, Chen K-F, Lin C, Cai L, Zhang H, et al. Upper critical solution temperature polymeric drug carriers. Chem Eng J 2022;432:134354. https://doi.org/10.1016/j.cej.2021.134354.
[120] Ansari MJ, Rajendran RR, Mohanto S, Agarwal U, Panda K, Dhotre K, et al. Poly(N-isopropylacrylamide)-based hydrogels for biomedical applications: a review of the state-of-the-art. Gels 2022;8:454. https://doi.org/10.3390/gels8070454.
[121] Shaibie NA, Ramli NA, Mohammad Faizal NDF, Srichana T, Mohd Amin MCI. Poly(N-isopropylacrylamide)-based polymers: recent overview for the development of temperature-responsive drug delivery and biomedical applications. Macromol Chem Phys 2023;224:2300157. https://doi.org/10.1002/macp.202300157.
[122] Tian L, Han S, Wu W, Li Z, He Z, Liu C, et al. Dose-effect relationship of copolymer on enhancing aqueous lubrication of a hybrid osteoarthritis drug delivery nanocarrier. J Colloid Interface Sci 2025;679:788–97. https://doi.org/10.1016/j.jcis.2024.10.162.
[123] Ghasemi S, Soltanimehr H, Rastegari B, Farjadian F. Multi-responsive nanocarrier based on P(NIPAM-*co*-DMAEA) grafted magnetic cellulose for controlled and targeted drug release. Int J Biol Macromol 2025;328:147417. https://doi.org/10.1016/j.ijbiomac.2025.147417.
[124] Wu W, Liu J, Lin X, He Z, Zhang H, Ji L, et al. Dual-functional MOFs-based hybrid microgel advances aqueous lubrication and anti-inflammation. J Colloid Interface Sci 2023;644:200–10. https://doi.org/10.1016/j.jcis.2023.04.071.
[125] Wu W, Liu J, Gong P, Li Z, Ke C, Qian Y, et al. Construction of core-shell NanoMOFs@microgel for aqueous lubrication and thermal-responsive drug release. Small 2022;18:2202510. https://doi.org/10.1002/smll.202202510.
[126] Tavagnacco L, Zaccarelli E, Chiessi E. On the molecular origin of the cooperative coil-to-globule transition of poly(N-isopropylacrylamide) in water. Phys Chem Chem Phys 2018;20:9997–10010. https://doi.org/10.1039/C8CP00537K.
[127] Yuan Y, Raheja K, Milbrandt N B, Beilharz S, Tene S, Oshabaheebwa S, et al. Thermoresponsive polymers with LCST transition: synthesis, characterization, and their impact on biomedical frontiers. RSC Appl Polym 2023;1:158–89. https://doi.org/10.1039/D3LP00114H.
[128] Liu M, Leroux J-C, Gauthier MA. Conformation–function relationships for the comb-shaped polymer pOEGMA. Prog Polym Sci 2015;48:111–21. https://doi.org/10.1016/j.progpolymsci.2015.03.001.
[129] Pires-Oliveira R, Tang J, Percebom AM, Petzhold CL, Tam KC, Loh W. Effect of molecular architecture and composition on the aggregation pathways of POEGMA random copolymers in water. Langmuir 2020;36:15018–29. https://doi.org/10.1021/acs.langmuir.0c02538.
[130] Dehghani B, Mirzaei M, Lohrasbi-Nejad A. Characterization of thermoresponsive poly(N-vinylcaprolactam) polymer containing doxorubicin-loaded niosomes: synthesis, structural properties, and anticancer efficacy. J Pharm Innov 2025;20:7. https://doi.org/10.1007/s12247-024-09913-y.
[131] Siirilä J, Häkkinen S, Tenhu H. The emulsion polymerization induced self-assembly of a thermoresponsive polymer poly(N - vinylcaprolactam). Polym Chem 2019;10:766–75. https://doi.org/10.1039/C8PY01421C.
[132] Makhaeva EE, Tenhu H, Khokhlov AR. Behavior of poly(N-vinylcaprolactam-co-methacrylic acid) macromolecules in aqueous solution: interplay between coulombic and hydrophobic interaction. Macromolecules 2002;35:1870–6. https://doi.org/10.1021/ma0105789.
[133] Cortez-Lemus NA, Licea-Claverie A. Poly(*N*-vinylcaprolactam), a comprehensive review on a thermoresponsive polymer becoming popular. Prog Polym Sci 2016;53:1–51. https://doi.org/10.1016/j.progpolymsci.2015.08.001.
[134] Rao KM, Rao KSVK, Ha C-S. Stimuli responsive poly(vinyl caprolactam) gels for biomedical applications. Gels Basel 2016;2:6. https://doi.org/10.3390/gels2010006.
[135] Lee JH, Yeo Y. Controlled drug release from pharmaceutical nanocarriers. Chem Eng Sci 2015;125:75–84. https://doi.org/10.1016/j.ces.2014.08.046.
[136] Ribeiro TP, Gomes FL, Vilarinho R, Salgado C, Martins MCL, Moreira JA, et al. Thermoresponsive nanoparticles for targeted and controlled delivery of doxorubicin in triple negative breast cancer: a 2D and 3D in vitro evaluation. Drug Deliv Transl Res 2025. https://doi.org/10.1007/s13346-025-01930-9.
[137] Paul DR. Elaborations on the Higuchi model for drug delivery. Int J Pharm 2011;418:13–7. https://doi.org/10.1016/j.ijpharm.2010.10.037.
[138] Peppas NA, Korsmeyer RW. Dynamically swelling hydrogels in Controlled release applications n.d.
[139] Peppas NA. A model of dissolution-controlled solute release from porous drug delivery polymeric systems. J Biomed Mater Res 1983;17:1079–87. https://doi.org/10.1002/jbm.820170615.
[140] Qian C, Mumby SJ, Eichinger BE. Phase diagrams of binary polymer solutions and blends. Macromolecules 1991;24:1655–61. https://doi.org/10.1021/ma00007a031.
[141] Cowen T, Karim K, Piletsky SA. Solubility and size of polymer nanoparticles. Polym Chem 2018;9:4566–73. https://doi.org/10.1039/C8PY00829A.
[142] Pontrelli G, Toniolo G, McGinty S, Peri D, Succi S, Chatgilialoglu C. Mathematical modelling of drug delivery from pH-responsive nanocontainers. Comput Biol Med 2021;131:104238. https://doi.org/10.1016/j.compbiomed.2021.104238.
[143] Sirousazar M. Mathematical modeling of drug release in a phase-transient temperature-responsive drug delivery system in spherical coordinates. J Macromol Sci Part B 2019;58:890–907. https://doi.org/10.1080/00222348.2019.1666528.
[144] Filippov SK, Khusnutdinov R, Murmiliuk A, Inam W, Zakharova LY, Zhang H, et al. Dynamic light scattering and transmission electron microscopy in drug delivery: A roadmap for correct characterization of nanoparticles and interpretation of results. Mater Horiz 2023;10:5354–70. https://doi.org/10.1039/D3MH00717K.
[145] Zhang S, Wang C. Precise analysis of nanoparticle size distribution in TEM image. Methods Protocols 2023;6:63. https://doi.org/10.3390/mps6040063.
[146] Zhang Q, Weber C, Schubert US, Hoogenboom R. Thermoresponsive polymers with lower critical solution temperature: from fundamental aspects and measuring techniques to recommended turbidimetry conditions. Mater Horiz 2017;4:109–16. https://doi.org/10.1039/C7MH00016B.
[147] Lou H, Hu G, Luan X, Steinbach-Rankins JM, Hageman MJ. Application of a UV-vis spectrometer to investigate the effect of dissolution media on the diffusivity of small molecules and proteins. J Pharm Sci 2025;114:256–64. https://doi.org/10.1016/j.xphs.2024.09.008.
[148] Kim Y, Park EJ, Kim TW, Na DH. Recent progress in drug release testing methods of biopolymeric particulate system. Pharmaceutics 2021;13:1313. https://doi.org/10.3390/pharmaceutics13081313.
[149] Veseli A, Žakelj S, Kristl A. A review of methods for solubility determination in biopharmaceutical drug characterization. Drug Dev Ind Pharm 2019;45:1717–24. https://doi.org/10.1080/03639045.2019.1665062.
[150] Demetzos C. Differential scanning calorimetry (DSC): A tool to study the thermal behavior of lipid bilayers and liposomal stability. J Liposome Res 2008;18:159–73. https://doi.org/10.1080/08982100802310261.
[151] Hahn A, Brandes G, Wagener P, Barcikowski S. Metal ion release kinetics from nanoparticle silicone composites. J Control Release 2011. https://doi.org/10.1016/j.jconrel.2011.05.023.
[152] Pu X-Q, Ju X-J, Zhang L, Cai Q-W, Liu Y-Q, Peng H-Y, et al. Novel multifunctional stimuli-responsive nanoparticles for synergetic chemo–photothermal therapy of tumors. ACS Appl Mater Interfaces 2021;13:28802–17. https://doi.org/10.1021/acsami.1c05330.
[153] Koochaki A, Moghbeli MR, Javan Nikkhah S. Coil-to-globule transition of thermo-responsive γ-substituted poly (ε-caprolactone) in water: A molecular dynamics simulation study. Curr Appl Phys 2018;18:1313–9. https://doi.org/10.1016/j.cap.2018.07.011.
[154] Füllbrandt M, Ermilova E, Asadujjaman A, Hölzel R, Bier FF, von Klitzing R, et al. Dynamics of linear poly(N-isopropylacrylamide) in water around the phase transition investigated by dielectric relaxation spectroscopy. J Phys Chem B 2014;118:3750–9. https://doi.org/10.1021/jp501325x.
[155] Fernandez-Rodriguez MA, Orozco-Barrera S, Sun W, Gámez F, Caro C, García-Martín ML, et al. Hot Brownian motion of thermoresponsive microgels in optical

tweezers shows discontinuous volume phase transition and bistability. Small Weinheim 2023;19:2301653. https://doi.org/10.1002/smll.202301653.
[156] Zhao C, Ma Z, Zhu XX. Rational design of thermoresponsive polymers in aqueous solutions: A thermodynamics map. Prog Polym Sci 2019;90:269–91. https://doi.org/10.1016/j.progpolymsci.2019.01.001.
[157] Pasparakis G, Tsitsilianis C. LCST polymers: Thermoresponsive nanostructured assemblies towards bioapplications. Polymer 2020;211:123146. https://doi.org/10.1016/j.polymer.2020.123146.
[158] Flory PJ. Thermodynamics of high polymer solutions. J Chem Phys 1942;10:51–61. https://doi.org/10.1063/1.1723621.
[159] Theory of solutions of high Polymers1, J Am Chem Soc n.d. https://pubs.acs.org/doi/abs/10.1021/ja01259a068 (accessed November 11, 2025).
[160] Hansen CM. Hansen solubility parameters: A user's handbook. 2nd ed. Boca Raton: CRC Press; 2007.
[161] Ethier JR, Antoniuk E, Brettmann B. Predicting polymer solubility from phase diagrams to compatibility: a perspective on challenges and opportunities. Soft Matter 2024;20:5652–69. https://doi.org/10.1039/D4SM00590B.
[162] Chang BH, Bae YC. Liquid–liquid equilibria of binary polymer solutions with specific interactions. Polymer 1998;39:6449–54. https://doi.org/10.1016/S0032-3861(97)10386-X.
[163] de Gennes PG. Dynamics of fluctuations and spinodal decomposition in polymer blends. J Chem Phys 1980;72:4756–63. https://doi.org/10.1063/1.439809.
[164] Cabral JT, Higgins JS. Spinodal nanostructures in polymer blends: on the validity of the Cahn-Hilliard length scale prediction. Prog Polym Sci 2018;81:1–21. https://doi.org/10.1016/j.progpolymsci.2018.03.003.
[165] Knychała P, Timachova K, Banaszak M, Balsara NP. 50th anniversary perspective: phase behavior of polymer solutions and blends. Macromolecules 2017;50:3051–65. https://doi.org/10.1021/acs.macromol.6b02619.
[166] Keßler S, Schmid F, Drese K. Modeling size controlled nanoparticle precipitation with the co-solvency method by spinodal decomposition. Soft Matter 2016;12:7231–40. https://doi.org/10.1039/C6SM01198E.
[167] Cahn JW. On spinodal decomposition. Acta Metall 1961;9:795–801. https://doi.org/10.1016/0001-6160(61)90182-1.
[168] Tanaka H. Viscoelastic phase separation. J Phys Condens Matter 2000;12:R207. https://doi.org/10.1088/0953-8984/12/15/201.
[169] Stetefeld J, McKenna SA, Patel TR. Dynamic light scattering: A practical guide and applications in biomedical sciences. Biophys Rev 2016;8:409–27. https://doi.org/10.1007/s12551-016-0218-6.
[170] Mochizuki K, Ben-Amotz D. Hydration-Shell transformation of thermosensitive aqueous polymers. J Phys Chem Lett 2017;8:1360–4. https://doi.org/10.1021/acs.jpclett.7b00363.
[171] Del Monte G, Truzzolillo D, Camerin F, Ninarello A, Chauveau E, Tavagnacco L, et al. Two-step deswelling in the volume phase transition of thermoresponsive microgels. Proc Natl Acad Sci USA 2021;118:e2109560118. https://doi.org/10.1073/pnas.2109560118.
[172] Fulton LA, Zhang P, Seitz WR, Tsavalas JG, Planalp RP. Dynamic aggregation of poly-N-Isopropylacrylamide characterized using second-order scattering. Appl Spectrosc 2018;72:1341–8. https://doi.org/10.1177/0003702818778601.
[173] Zahednezhad F, Allahyari S, Sarfraz M, Zakeri-Milani P, Feyzizadeh M, Valizadeh H. Liposomal drug delivery systems for organ-specific cancer targeting: early promises, subsequent problems, and recent breakthroughs. Expert Opin Drug Deliv 2024;21:1363–84. https://doi.org/10.1080/17425247.2024.2394611.
[174] Basak S, Das TK, Basak S, Das TK. Liposome-based drug delivery systems: From laboratory research to industrial production—instruments and challenges. ChemEngineering 2025;9. https://doi.org/10.3390/chemengineering9030056.
[175] Bi H, Xue J, Jiang H, Gao S, Yang D, Fang Y, et al. Current developments in drug delivery with thermosensitive liposomes. Asian J Pharm Sci 2019;14:365–79. https://doi.org/10.1016/j.ajps.2018.07.006.
[176] Maritim S, Boulas P, Lin Y. Comprehensive analysis of liposome formulation parameters and their influence on encapsulation, stability and drug release in glibenclamide liposomes. Int J Pharm 2021;592:120051. https://doi.org/10.1016/j.ijpharm.2020.120051.
[177] Liu P, Chen G, Zhang J. A review of liposomes as a drug delivery system: current status of approved products, regulatory environments, and future perspectives. Molecules 2022;27:1372. https://doi.org/10.3390/molecules27041372.
[178] Pande S. Factors affecting response variables with emphasis on drug release and loading for optimization of liposomes. Artif Cells Nanomed Biotechnol 2024;52:334–44. https://doi.org/10.1080/21691401.2024.2360634.
[179] Gabizon AA, Gabizon-Peretz S, Modaresahmadi S, La-Beck NM. Thirty years from FDA approval of pegylated liposomal doxorubicin (Doxil/Caelyx): An updated analysis and future perspective. BMJ Oncol 2025;4:e000573. https://doi.org/10.1136/bmjonc-2024-000573.
[180] Mohamed M, Alaaeldin E, Hussein AA, Sarhan H. Liposomes and PEGylated liposomes as drug delivery system. J Adv Biomed Pharm Sci 2020;3:80–8. https://doi.org/10.21608/jabps.2020.22937.1068.
[181] Maurelli AM, De Leo V, Catucci L. Polydopamine-modified liposomes: preparation and recent applications in the biomedical field. ACS Omega 2024;9:24105–20. https://doi.org/10.1021/acsomega.4c02555.
[182] Cao Y, Dong X, Chen X. Polymer-modified liposomes for drug delivery: from fundamentals to applications. Pharmaceutics 2022;14:778. https://doi.org/10.3390/pharmaceutics14040778.
[183] Shah S, Famta P, Raghuvanshi RS, Singh SB, Srivastava S. Lipid polymer hybrid nanocarriers: insights into synthesis aspects, characterization, release mechanisms, surface functionalization and potential implications. Colloid Interface Sci Commun 2022;46:100570. https://doi.org/10.1016/j.colcom.2021.100570.
[184] Harvey S, Austin J, Bancarz D, Malm A. A thermally robust method of sample sealing for capillary DLS. MethodsX 2023;10:102142. https://doi.org/10.1016/j.mex.2023.102142.
[185] Monge S, Antoniacomi S, Lapinte V, Darcos V, Robin J-J. Poly(tris (hydroxymethyl)acrylamidomethane)-based copolymers: A new class of acid-labile thermosensitive polymers. Polym Chem 2012;3:2502–7. https://doi.org/10.1039/C2PY20309J.
[186] Gan Z, Fung JT, Jing X, Wu C, Kuliche WK. A novel laser light-scattering study of enzymatic biodegradation of poly(ε-caprolactone) nanoparticles. Polymer 1999;40:1961–7. https://doi.org/10.1016/S0032-3861(98)00414-5.
[187] Farkas N, Kramar JA. Dynamic light scattering distributions by any means. J Nanopart Res 2021;23:120. https://doi.org/10.1007/s11051-021-05220-6.
[188] Watt J, Huber DL, Stewart PL. Soft matter and nanomaterials characterization by cryogenic transmission electron microscopy. MRS Bull 2019;44:942–8. https://doi.org/10.1557/mrs.2019.285.
[189] Pandey N, Menon JU, Takahashi M, Hsieh J-T, Yang J, Nguyen KT, et al. Thermo-responsive fluorescent nanoparticles for multimodal imaging and treatment of cancers. Nanotheranostics 2020;4:1–13. https://doi.org/10.7150/ntno.39810.
[190] Baidurah S. Methods of analyses for biodegradable polymers: A review. Polymers 2022;14:4928. https://doi.org/10.3390/polym14224928.
[191] Kochovski Z, Chen G, Yuan J, Lu Y. Cryo-Electron microscopy for the study of self-assembled poly(ionic liquid) nanoparticles and protein supramolecular structures. Colloid Polym Sci 2020;298:707–17. https://doi.org/10.1007/s00396-020-04657-w.
[192] Monnier CA, Thévenaz DC, Balog S, Fiore GL, Vanhecke D, Rothen-Rutishauser B, et al. A guide to investigating colloidal nanoparticles by cryogenic transmission electron microscopy: pitfalls and benefits. AIMS Biophys 2015;2:245–58. https://doi.org/10.3934/biophy.2015.3.245.
[193] Karjalainen E, Aseyev V, Tenhu H. Influence of hydrophobic anion on solution properties of PDMAEMA. Macromolecules 2014;47:2103–11. https://doi.org/10.1021/ma5000706.
[194] Constantinou AP, Wang L, Wang S, Georgiou TK. Thermoresponsive block copolymers of increasing architecture complexity: A review on structure–property relationships. Polym Chem 2023;14:223–47. https://doi.org/10.1039/D2PY01097F.
[195] Yusefi M, Soon ML-K, Teow S-Y, Monchouguy EI, Neerooa BNHM, Izadiyan Z, et al. Fabrication of cellulose nanocrystals as potential anticancer drug delivery systems for colorectal cancer treatment. Int J Biol Macromol 2022;199:372–85. https://doi.org/10.1016/j.ijbiomac.2021.12.189.
[196] Rakhshaei R, Namazi H, Hamishehkar H, Rahimi M. Graphene quantum dot cross-linked carboxymethyl cellulose nanocomposite hydrogel for pH-sensitive oral anticancer drug delivery with potential bioimaging properties. Int J Biol Macromol 2020;150:1121–9. https://doi.org/10.1016/j.ijbiomac.2019.10.118.
[197] Varela-Moreira A, van Leur H, Krijgsman D, Ecker V, Braun M, Buchner M, et al. Utilizing *in vitro* drug release assays to predict *in vivo* drug retention in micelles. Int J Pharm 2022;618:121638. https://doi.org/10.1016/j.ijpharm.2022.121638.
[198] Weng J, Tong HHY, Chow SF. In vitro release study of the polymeric drug nanoparticles: development and validation of a novel method. Pharmaceutics 2020;12:732. https://doi.org/10.3390/pharmaceutics12080732.
[199] Yu M, Yuan W, Li D, Schwendeman A, Schwendeman SP. Predicting drug release kinetics from nanocarriers inside dialysis bags. J Control Release 2019;315:23–30. https://doi.org/10.1016/j.jconrel.2019.09.016.
[200] Wallenwein CM, Nova MV, Janas C, Jablonka L, Gao GF, Thurn M, et al. A dialysis-based *in vitro* drug release assay to study dynamics of the drug-protein transfer of temoporfin liposomes. Eur J Pharm Biopharm 2019;143:44–50. https://doi.org/10.1016/j.ejpb.2019.08.010.
[201] D'Souza S. A review of in vitro drug release test methods for nano-sized dosage forms. Adv Pharm 2014;2014:304757. https://doi.org/10.1155/2014/304757.
[202] Baka E, Comer JEA, Takács-Novák K. Study of equilibrium solubility measurement by saturation shake-flask method using hydrochlorothiazide as model compound. J Pharm Biomed Anal 2008;46:335–41. https://doi.org/10.1016/j.jpba.2007.10.030.
[203] Chiu MH, Prenner EJ. Differential scanning calorimetry: An invaluable tool for a detailed thermodynamic characterization of macromolecules and their interactions. J Pharm Bioallied Sci 2011;3:39–59. https://doi.org/10.4103/0975-7406.76463.
[204] Sun L, Böckmann RA. Membrane phase transition during heating and cooling: molecular insight into reversible melting. Eur Biophys J 2018;47:151–64. https://doi.org/10.1007/s00249-017-1237-3.
[205] Fahmy MA. A computational model for nonlinear biomechanics problems of FGA biological soft tissues. Appl Sci 2022;12:7174. https://doi.org/10.3390/app12147174.
[206] Adabbo G, Andreozzi A, Iasiello M, Vanoli GP. Numerical evaluation of heat-triggered drug release via thermo-sensitive liposomes: A comparison between image-based vascularized tumor and volume-averaged porous media models. Int J Heat Mass Transf 2024;220:124942. https://doi.org/10.1016/j.ijheatmasstransfer.2023.124942.
[207] Moradi Kashkooli F, Souri M, Tavakkoli JJ, C Kolios M. A spatiotemporal computational model of focused ultrasound heat-induced nano-sized drug delivery system in solid tumors. Drug Deliv 2023;30:2219871. https://doi.org/10.1080/10717544.2023.2219871.
[208] Koutsi M, Mpekris F, Stylianopoulos T. A multiphysics computational model of focused ultrasound-enhanced drug delivery using temperature-sensitive liposomes. 2025. https://doi.org/10.21203/rs.3.rs-8143174/v1.

[209] Martineau RL, Bayles AV, Hung C-S, Reyes KG, Helgeson ME, Gupta MK. Engineering gelation kinetics in living silk hydrogels by differential dynamic microscopy microrheology and machine learning. Adv Biol 2022;6:2101070. https://doi.org/10.1002/adbi.202101070.
[210] Seifermann M, Reiser P, Friederich P, Levkin PA. High-throughput synthesis and machine learning assisted design of photodegradable hydrogels. Small Methods 2023;7:2300553. https://doi.org/10.1002/smtd.202300553.
[211] Gao XJ, Ciura K, Ma Y, Mikolajczyk A, Jagiello K, Wan Y, et al. Toward the integration of machine learning and molecular modeling for designing drug delivery nanocarriers. Adv Mater 2024;36:2407793. https://doi.org/10.1002/adma.202407793.
[212] Tao H, Wu T, Aldeghi M, Wu TC, Aspuru-Guzik A, Kumacheva E. Nanoparticle synthesis assisted by machine learning. Nat Rev Mater 2021;6:701–16. https://doi.org/10.1038/s41578-021-00337-5.
[213] Ejeromedoghene O, Kumi M, Akor E, Zhang Z. The application of machine learning in 3D/4D printed stimuli-responsive hydrogels. Adv Colloid Interf Sci 2025;336:103360. https://doi.org/10.1016/j.cis.2024.103360.
[214] Lin Z, Chou W-C, Cheng Y-H, He C, Monteiro-Riviere NA, Riviere JE. Predicting nanoparticle delivery to tumors using machine learning and artificial intelligence approaches. Int J Nanomedicine 2022;17:1365–79. https://doi.org/10.2147/IJN.S344208.
[215] Chou W-C, Chen Q, Yuan L, Cheng Y-H, He C, Monteiro-Riviere NA, et al. An artificial intelligence-assisted physiologically-based pharmacokinetic model to predict nanoparticle delivery to tumors in mice. J Control Release 2023;361:53–63. https://doi.org/10.1016/j.jconrel.2023.07.040.
[216] Mi K, Chou W-C, Chen Q, Yuan L, Kamineni VN, Kuchimanchi Y, et al. Predicting tissue distribution and tumor delivery of nanoparticles in mice using machine learning models. J Control Release 2024;374:219–29. https://doi.org/10.1016/j.jconrel.2024.08.015.
[217] Bilgi E, Winkler DA, Oksel Karakus C. Identifying factors controlling cellular uptake of gold nanoparticles by machine learning. J Drug Target 2024;32:66–73. https://doi.org/10.1080/1061186X.2023.2288995.
[218] Debnath G, Vasu B, Gorla RSR. Current state-of-the-art in multi-scale modeling in nano-cancer drug delivery: role of AI and machine learning. Cancer Nanotechnol 2025;16:45. https://doi.org/10.1186/s12645-025-00326-1.
[219] Hopkins SD, Blaisten-Barojas E. Molecular dynamics simulations evidence the thermoresponsive behavior of PNIPAM and PDEA in glycerol solutions. Front Nanotechnol 2023:5. https://doi.org/10.3389/fnano.2023.1292259.
[220] Tavagnacco L, Zaccarelli E, Chiessi E. Modeling solution behavior of poly(N-isopropylacrylamide): A comparison between water models. J Phys Chem B 2022;126:3778–88. https://doi.org/10.1021/acs.jpcb.2c00637.
[221] Chen X, Niu D, Gao H, Du M. Molecular dynamics study on hydrothermal response of PNIPAM: from single chain to cross-linked polymer. FHMT 2024;22:1743–60. https://doi.org/10.32604/fhmt.2024.058274.